

Intramolecularly Coordinated (6-(Diphenylphosphino)acenaphth-5-yl)stannanes. Repulsion vs Attraction of P- and Sn-Containing Substituents in the *peri* Positions

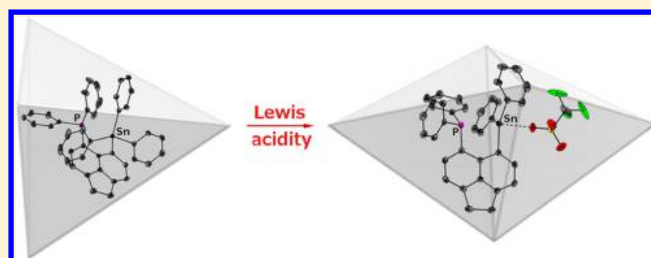
Emanuel Hupf,[†] Enno Lork,[†] Stefan Mebs,^{*,‡} and Jens Beckmann^{*,†}

[†]Institut für Anorganische Chemie, Universität Bremen, Leobener Straße, 28359 Bremen, Germany

[‡]Institut für Chemie und Biochemie, Freie Universität Berlin, Fabeckstraße 36a, 14195 Berlin, Germany

Supporting Information

ABSTRACT: The intramolecularly coordinated (6-(diphenylphosphino)acenaphth-5-yl)stannanes ArSnBu₃ (1), ArSnPh₃ (2), ArSnPh₂Cl (3), ArSnPhCl₂ (4), ArSnCl₃ (5), Ar₂SnCl₂ (6), ArSnPh₂O₃SCF₃ (7), and ArSnPh₂F (8) were synthesized and fully characterized by multinuclear NMR spectroscopy (¹¹⁹Sn, ³¹P, ¹⁹F, ¹³C, ¹H) and X-ray crystallography (Ar = 6-Ph₂P-Ace-5-). Due to the different substituents, the Lewis acidities of the Sn atoms of 1–8 vary substantially, which is reflected in the different P–Sn *peri* distances lying in the range from 2.7032(9) to 3.332(2) Å. In MeCN, 7 undergoes electrolytic dissociation into solvated triarylstannyl cations and triflate anions. The gas-phase structures of 2–5, 8, and the triarylstannyl cations ArPh₂Sn⁺ (7a) and [ArPh₂Sn·NCMe]⁺ (7b) were obtained by geometry optimization at the B3PW91/TZ level of theory. A detailed analysis of a set of real-space bonding indicators (RSBI) derived from the electron and pair densities following the atoms in molecules (AIM) and electron localizability indicator (ELI-D) topological approaches, respectively, uncovers the Sn–P *peri* interaction in 2 to be in the border regime between nonbonding and weakly ionic. With an increasing number of Cl atoms attached to the Sn atom, the Sn–P bond becomes considerably shorter and exhibits a decreasingly polar covalent interaction. As expected, this trend is significantly enhanced for the Sn–P interactions in the charged compounds 7a,b. The Sn–P bond properties of 8, however, very much resemble those of 3, which means that the electronic impact of the F atom in the axial position is comparable to that of the axial Cl atom.



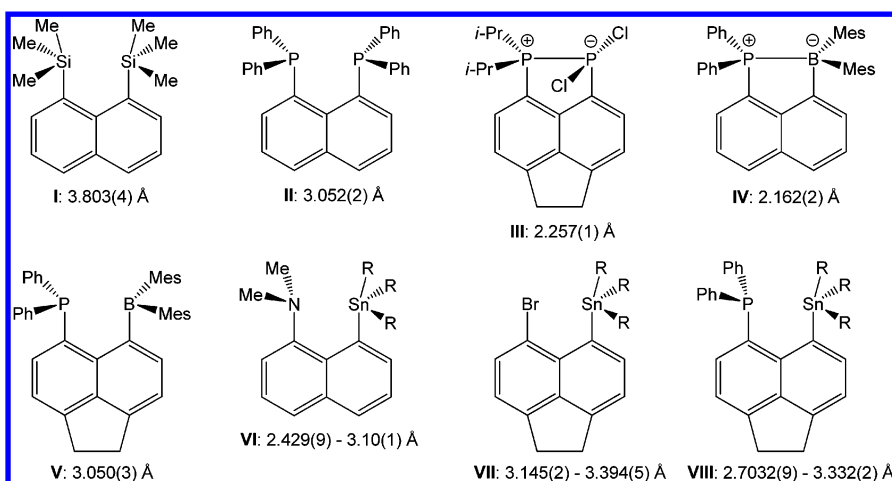
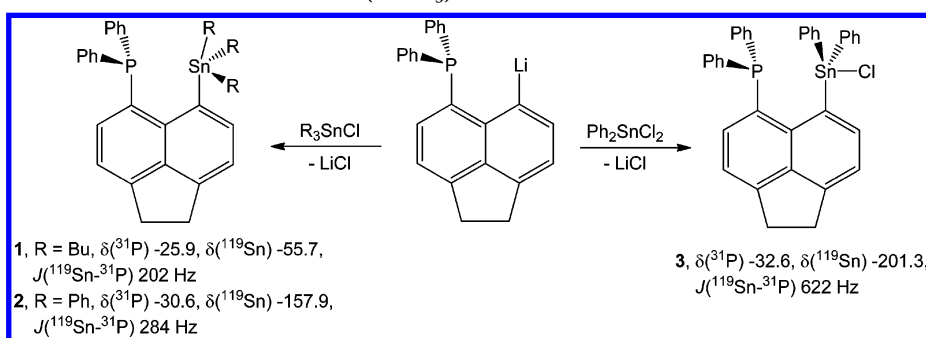
INTRODUCTION

Peri-substituted naphthalenes (Nap) and acenaphthenes (Ace) feature constrained interactions between the substituents in 1,8- and 5,6-positions that can be either repulsive due to steric congestion or attractive due to weak or strong bonding.¹ With few exceptions, the *peri* interactions were analyzed solely by the inspection of geometrical bond parameters, which provide a good impression of the (non)bonding character for clear-cut cases. 1,8-Bis(trimethylsilyl)naphthalene (I; 1,8-(Me₃Si)₂-Nap), possessing an extremely long *peri* distance (3.803(4) Å), is a compelling example for strongly repulsive interactions (Scheme 1).² 1,8-Bis(diphenylphosphino)naphthalene (II; 1,8-(Ph₂P)₂-Nap) is another straightforward case in which the two lone pairs impose repulsion, leading to a moderately long *peri* distance (3.052(2) Å).³ In contrast, the related 5-(dichlorophosphino)-6-(diisopropylphosphino)acenaphthene (III; 5-(Cl₂P)-6-(i-Pr₂P)-Ace) gives rise to a short *peri* distance (2.257(1) Å) due to the different substituents attached to the P atoms, pointing to a strongly attractive interaction.⁴

In (1-(diphenylphosphino)naphth-8-yl)dimesitylborane (IV; 1-(Ph₂P)-8-(Mes₂B)-Nap) the combination of a donor and an acceptor atom affords a Lewis pair with a short *peri* distance (2.162(2) Å) that is indicative of a strongly attractive

interaction (Scheme 1).^{5,6} However, the closely related (5-(diphenylphosphino)acenaphth-6-yl)dimesitylborane (V; 5-(Ph₂P)-6-(Mes₂B)-Ace) comprises a frustrated Lewis pair (FLP) with a long *peri* distance (3.050(3) Å).⁶ In this case the predominantly repulsive interaction stems from the conformational rigidity of the acenaphthene moiety, which outweighs the attraction between the donor and the acceptor atoms. For the heavier heteroatoms the steric congestion will arguably increase along with the covalent radii; however, the consequences for the nature of the interactions are not apparent. With the elongation of the heteroatom–carbon bond the conformational flexibility will also increase, which might in fact reduce the repulsion between the *peri* substituents.⁷ (8-(Dimethylamino)naphthyl)stannanes R₃Sn-8-Me₂N-Nap (VI)⁸ and 6-(bromoacenaphth-5-yl)stannanes 5-R₃Sn-6-Br-Ace (VII)⁹ are significant subclasses of heavily substituted naphthalenes and acenaphthenes, in which the N–Sn and Br–Sn *peri* interactions are indisputable due to the ¹¹⁹Sn NMR chemical shifts, which are indicative of hypercoordinated Sn atoms (R = Cl, Br, I, alkyl, aryl). In general,

Received: February 12, 2014

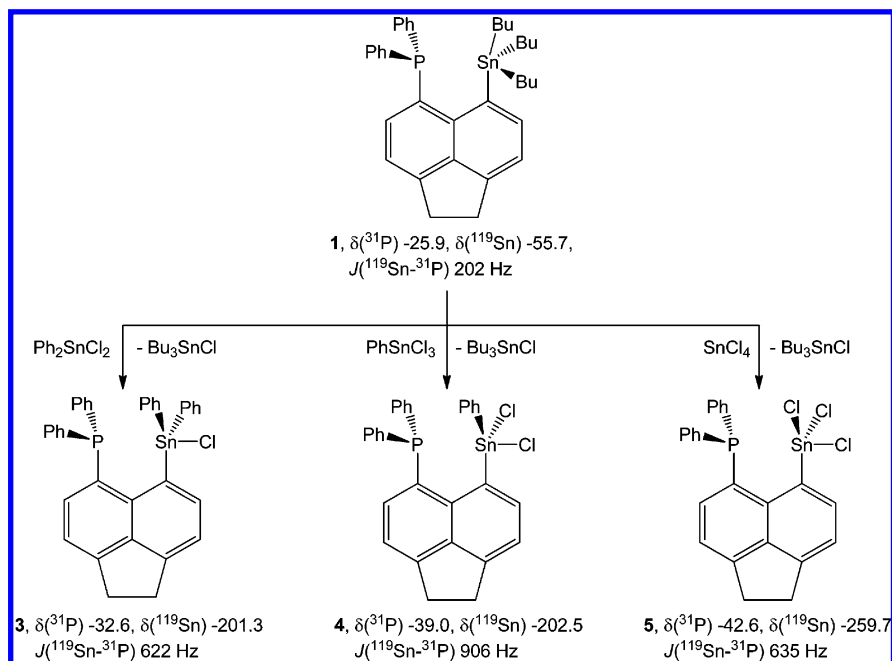
Scheme 1. *peri*-Substituted Naphthalenes I, II, IV, and VI as well as Acenaphthenes III, V, VII, and VIII and Selected *peri* DistancesScheme 2. Synthesis and Selected NMR Parameters (CDCl_3) of 1–3

intramolecularly coordinated organostannanes containing N and O donor atoms have received tremendous interest in the last three decades,^{10–12} e.g. due to their relevance as isolable intermediates of substitution reactions. In a classic paper, Britton and Dunitz investigated the structural correlation of pentacoordinated organostannanes with the trajectory of the $\text{S}_{\text{N}}2$ reaction pathway.¹³ Although it has been recently challenged, a simplistic bond model describes the axial substituents of the trigonal bipyramid, representing the entering group and the leaving group, as three-center–four-electron (3c–4e) bonds involving the p_z orbital of the Sn atom.¹⁴ Bonding of the three equatorial substituents of the group 14 element has been attributed to three sp^2 orbitals. At the preliminary stage of the $\text{S}_{\text{N}}2$ reaction pathway often complexes weakly associated with the entering group are formed, in which the sp^3 hybridization of the group 14 compound is still retained. These interactions are commonly referred to as σ -hole bonding.¹⁵ The *peri* distances of compound classes VI and VII vary within a large range (2.426(9)–3.394(5) Å). Whether or not these *peri* interactions are attractive or even repulsive is ambiguous and might greatly depend on the Lewis acidity, which in turn is influenced by the three remaining substituents attached to the Sn atoms. For those cases the sole inspection of the molecular geometries cannot provide an insight into the bonding character. This holds particularly true for the transition from a nonbonding state to a weakly coordinating state. Detailed bonding information can be obtained by means of computational chemistry. However, standard calculation of the molecular wave function and subsequent analysis of the molecular orbitals (MO) and/or natural bond orbitals

(NBO) often fail to provide a clear picture for the heavier elements, particularly when the interactions involved are weak.

Another approach entails topological analysis of the electron densities (ED) according to the atoms in molecules (AIM) theory,¹⁶ which affords reliable atomic properties such as charges and volumes as well as bonding properties in terms of so-called bond critical points (bcp). The ED can be extracted from the calculated wave functions but also determined experimentally by high-resolution X-ray diffraction of the solid-state structures, which is an advantage over all other theoretical methods.¹⁷ A complementary set of bonding descriptors is provided by topological analysis of the corresponding electron pair densities according to the electron localization function¹⁸ (ELF) or the more advanced electron localizability indicator (ELI-D).¹⁹ Both concepts divide space into basins of localized electron pairs (e.g. bonding basins, lone pairs) and can only be obtained from theoretical calculations. In this study, the ELI-D is applied. A tool for estimation of bond polarities is the Raub–Jansen index (RJI),²⁰ which was invented for the ELF but was also later used for the ELI-D (to discriminate dative bonds from polar-covalent interactions).²¹ With this tool the electron population within an ELF/ELI-D bonding basin connecting two or more atoms is fragmented into particular contributions of the two or more AIM atomic basins enclosing this bond. For a homopolar bond the RJI equals 50% and it increases with increasing bond polarity.

In this work we describe the synthesis and characterization of a series of (6-(diphenylphosphino)acenaphth-5-yl)stannanes 5- R_3Sn -6- Ph_2P -Ace (VIII), whereby we varied the nature of the

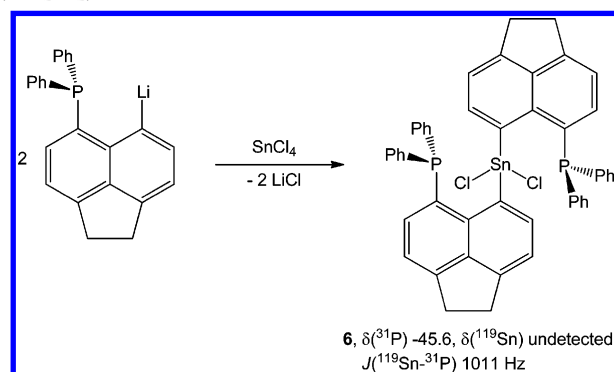
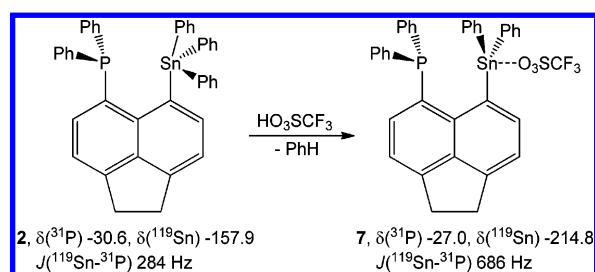
Scheme 3. Synthesis and Selected NMR Parameters (CDCl_3) of 3–5

substituents ($\text{R} = \text{Bu}, \text{Ph}, \text{Cl}, \text{O}_3\text{SCF}_3, \text{F}$).²² The characterization was achieved by multinuclear NMR spectroscopy (^{119}Sn , ^{31}P , ^{19}F , ^{13}C , ^1H) and X-ray crystallography. Real-space bonding descriptors were derived from AIM and ELI-D analyses of selected gas-phase structures optimized at the B3PW91/TZ level of theory, which unraveled the bond character of the P–Sn *peri* interactions.

RESULTS AND DISCUSSION

Synthetic Aspects. The reaction of 5-bromo-6-(diphenylphosphino)acenaphthene (ArBr) with *n*-butyllithium and *N,N,N',N'*-tetramethylethylenediamine (TMEDA) at -78°C proceeded with facile metal halide exchange and gave rise to the formation of the corresponding lithium organyl ArLi ($\text{Ar} = 6\text{-Ph}_2\text{P-Ace-5-}$). The subsequent salt metathesis reaction with tributyltin chloride, triphenyltin chloride, and diphenyltin dichloride at room temperature provided (6-(diphenylphosphino)acenaphth-5-yl)tributyltin (**1**; ArSnBu_3), (6-(diphenylphosphino)acenaphth-5-yl)triphenyltin (**2**; ArSnPh_3), and (6-(diphenylphosphino)acenaphth-5-yl)diphenyltin chloride (**3**; ArSnPh_2Cl), which were isolated in 71%, 74%, and 35% yields, respectively (Scheme 2).

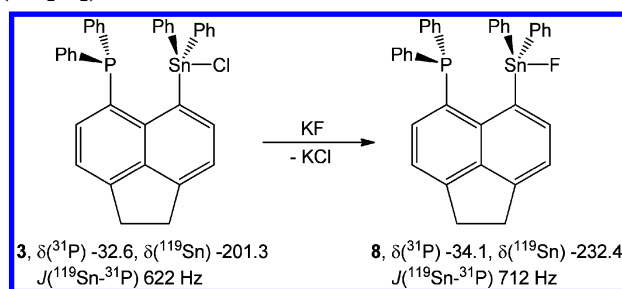
The aryltributylstannane **1** proved to be a precursor for the transmetalation reaction with diphenyltin dichloride, phenyltin trichloride, and tin(IV) chloride, affording (6-(diphenylphosphino)acenaphth-5-yl)diphenyltin chloride (**3**; ArSnPh_2Cl), (6-(diphenylphosphino)acenaphth-5-yl)phenyltin dichloride (**4**; ArSnPhCl_2), and (6-(diphenylphosphino)acenaphth-5-yl)tin trichloride (**5**; ArSnCl_3) in 15%, 85%, and 97% yields, respectively (Scheme 3). The reaction of the lithium organyl ArLi with tin tetrachloride at -78°C at a molar ratio of 1:2 produced the disubstituted product bis(6-(diphenylphosphino)acenaphth-5-yl)tin dichloride (**6**; Ar_2SnCl_2) in 14% yield (Scheme 4). Treatment of ArSnPh_3 (**2**) with triflic acid provided (6-(diphenylphosphino)acenaphth-5-yl)diphenylstannyl triflate (**7**; $\text{ArSnPh}_2\text{O}_3\text{SCF}_3$) after recrystallization in 40% yield (Scheme 5).

Scheme 4. Synthesis and Selected NMR Parameters (CD_2Cl_2) of 6Scheme 5. Synthesis and Selected NMR Parameters (CDCl_3) of 7

The reaction of ArSnPh_2Cl (**3**) with KF in DMF proceeded with chloride/fluoride exchange and gave rise to the formation of (6-(diphenylphosphino)acenaphth-5-yl)diphenyltin fluoride (**8**; ArSnPh_2F) in 89% yield (Scheme 6). Compounds **1–8** were obtained as colorless crystals that are, with the exception of **5**, reasonably stable toward moist air.

Solid-State Structures. The molecular structures of **1–8** established by X-ray crystallography are shown in Figure 1. The first coordination sphere of the Sn atoms is defined by C_4 , C_3Cl , C_2Cl_2 , CCl_3 , C_3O , and C_3F donor sets. Related bond

Scheme 6. Synthesis and Selected NMR Parameters (CD_2Cl_2) of **8**



parameters are collected in Table 1. The second coordination sphere of the Sn atoms contains the P atoms situated across the bay region of the acenaphthene moieties. Geometric parameters associated with the P–Sn *peri* substitution are given in Table 2. The spatial arrangement of the Sn atoms of **1–5**, **7**, and **8** lies between a tetrahedron and a trigonal bipyramid (coordination number 4 + 1), whereby the C and Cl atoms are situated in the equatorial positions. The axial positions are occupied by P atoms and C atoms (**1**, **2**), Cl atoms (**3–5**), an O atom (**7**), and a F atom (**8**).

The geometrical goodness (definition $\Delta\sum(\theta) = \sum(\theta_{\text{eq}}) - \sum(\theta_{\text{ax}})$; 0° (tetrahedron) $\leq \Delta\sum(\theta) \leq 90^\circ$ (trigonal bipyramid))²³ mostly depends on the second axial atom (C, Cl, O, F) and ranges from $\Delta\sum(\theta) = 33.1^\circ$ (**1**) and 25.6° (**2**) over 69.2° (**8**), 69.7° (**4**), 73.3° (**5**), and 74.6° (**3**) to the maximum value of 92.1° (**7**). Notably, the low $\Delta\sum(\theta)$ values of **1** and **2** may represent the bonding situation at the early stage of the $\text{S}_{\text{N}}2$ reaction pathway, which has been denoted as σ -hole bonding,¹⁵ whereas the high $\Delta\sum(\theta)$ value of **7** may related to a pentacoordinated intermediate in which the entering group and the leaving group are almost equally bonded.¹⁴ The spatial arrangement of the Sn atom of **6** is distorted octahedral (coordination number 4 + 2). The Sn–C and Sn–Cl bond lengths of **1–8** are inconspicuous and resemble values found in other tetra-, penta-, or hexacoordinated organotin compounds. The Sn...O bond length of **7** (2.391(3) Å) is expectedly longer than the “standard” Sn–O bond length of Mes_3SnOH (1.999(6) Å)²⁴ and accounts for a Pauling bond order (definition $\log \text{BO} = -c(d - d_{\text{st}})$; $c = 1.41$, $d_{\text{st}} = 2.00$)²⁵ of $\text{BO} = 0.28$. These values are consistent with weak ion pairing between the triorganotin cation and the triflate anion of **7** and compare well with those of other triorganotin triflates such as the polymeric $\text{Ph}_3\text{SnO}_3\text{SCF}_3$ (2.375(4) and 2.310(4) Å; $\text{BO} = 0.30$ and 0.37)²⁶ and the monomeric $[(\text{Me}_3\text{Si})_2\text{CH}]_3\text{SnO}_3\text{SCF}_3$ (2.139(4) Å; $\text{BO} = 0.64$).²⁷ The Sn–F bond length of **8** (2.005(6) Å) lies about midway between those of the monomeric Mes_3SnF (1.957(4) and 1.965(4) Å)²⁴ containing tetracoordinated Sn atoms and the polymeric Ph_3SnF (2.1458(3))²⁸ containing pentacoordinated Sn atoms. It compares best with the triphenyldifluorostannate ion $[\text{Ph}_3\text{SnF}_2]^-$ (2.072(4) Å)²⁹ containing also pentacoordinated Sn atoms. The P–Sn *peri* distances of aryltin(IV) species **1–8** vary between 2.7032(9) Å (**7**) and 3.332(2) Å (**1**) and are therefore larger than that of the recently published diarylstannylene 5-(2',4',6'-*i*-Pr₃C₆H₃Sn)-6-(*i*-Pr₂P)-Ace (2.6362(6) Å).³⁰ Within the series of pentacoordinated $\text{ArSnPh}_{3-n}\text{Cl}_n$ species **2** ($n = 0$; 3.247(2) Å), **3** ($n = 1$; 2.9075(6) Å), **4**, ($n = 2$; 2.855(2) Å), and **5** ($n = 3$; 2.757(2) Å) the P–Sn *peri* distance decreases with an increasing number of chlorine atoms, reflecting the growing Lewis acidity of the Sn atoms (Ar

= 6-Ph₂P-Ace-5). The P–Sn *peri* distance of 2.918(2) Å for the hexacoordinated **6** lies about midway between the values of **2** and **3**. Within the series ArSnPh_2X the P–Sn *peri* distance decreases with the decreasing donor strength of the group X when going from **2** (X = Ph; 3.247(2) Å) over **8** (X = F; 2.937(3) Å) and **3** (X = Cl; 2.9075(6) Å) to **7** (X = O₃SCF₃; 2.7032(9) Å), pointing to a *trans* effect of the axial substituents. The splay angle (definition $\sum(\text{three bay region angles}) - 360^\circ$)⁹ correlates well with the P–Sn *peri* distances and decreases from 19.0° (**1**) to 2.9° (**7**); however, the out-of-plane displacements of the Sn and P atoms appear not to follow a trend (Table 2).

Structures in Solution. With the exception of **6**, **1–8** are reasonably soluble in moderately polar solvents such as CHCl_3 and THF. In these solvents **1–8** are nonelectrolytes, as the conductivity is below the detection limit. The triaryltin triflate **7** is also soluble in MeCN, in which it undergoes electrolytic dissociation into solvated triarylstannyl and triflate ions. The molar conductivity (MeCN , $c = 5 \times 10^{-7}$ mol L⁻¹) of **7** ($\Lambda = 360 \Omega^{-1} \text{cm}^2 \text{mol}^{-1}$) is in agreement with the presence of 1/1 electrolytes.³¹ The ³¹P NMR and ¹¹⁹Sn NMR chemical shifts of **7** in CDCl_3 (δ -27.0/-214.8) and in MeCN (δ -24.4/-194.8) are distinctively different, but both are in the expected range of tetracoordinated P and pentacoordinated Sn atoms. The ¹¹⁹Sn NMR chemical shift of an unsolvated tetracoordinated triaryltin cation would be expected to be substantially shifted to low field. The reasonably similar $J(^{31}\text{P}-^{119}\text{Sn})$ couplings in CDCl_3 (686 Hz) and MeCN (585 Hz) support the assumption that the triarylstannyl cation is solvated by MeCN. It should be noted, however, that the MeCN is lost under ESI MS conditions ($\text{CH}_2\text{Cl}_2/\text{MeCN}$ 1/10), as only the mass cluster at m/z 611.3 indicative of the unsolvated $[\text{5}-(\text{SnPh}_2)\text{-6}-(\text{Ph}_2\text{P})\text{Ace}]^+$ was observed. Within the series of pentacoordinated $\text{ArSnPh}_{3-n}\text{Cl}_n$ species the ¹¹⁹Sn NMR chemical shifts (CDCl_3) are consecutively shifted to high field when going from **2** ($n = 0$; δ -157.9) over **3** ($n = 1$; δ -200.8) and **4** ($n = 2$; δ -202.5) to **5** ($n = 3$; δ -259.7), indicating the increasing coordination number of the Sn atoms. All of these ¹¹⁹Sn NMR signals are shifted more to high field than those of the phenylstannanes Ph_4Sn (δ -131), Ph_3SnCl (δ -48), Ph_2SnCl_2 (δ -32), and PhSnCl_3 (δ -63), lacking an intramolecular donor substituent.³² Within the same series of pentacoordinated species the ³¹P NMR chemical shifts (CDCl_3) are also consecutively shifted to high field when going from **2** ($n = 0$; δ -30.6) over **3** ($n = 1$; δ -33.2) and **4** ($n = 2$; δ -39.0) to **5** ($n = 3$; δ -42.6). The hexacoordinated Ar_2SnCl_2 species **6** possesses the most high field shifted ³¹P NMR signal (-45.6), while no ¹¹⁹Sn NMR signal was obtained due to its low solubility. The very different $J(^{119}\text{Sn}-^{31}\text{P})$ coupling constants of **1–8**, ranging from 202 to 1011 Hz, deserve particular attention.

In cases where the Sn and P atoms are formally nonbonded, the observed coupling constant might be a combination of a through-space coupling and a dipole–dipole coupling mediated through the four bonds of the acenaphthyl framework. In cases where the Sn and P atoms are covalently bonded, the observed coupling constant might be due to the sum of two dipole–dipole couplings, namely, a larger ¹*J* coupling and a substantially smaller ⁴*J* coupling, which can be of the same or opposite sign. For weak donor–acceptor interactions and the onset of three-center–four-electron (3c-4e) axial bonding the situation is ambiguous.³³ There is no simple numeric correlation of the $J(^{119}\text{Sn}-^{31}\text{P})$ coupling constants with the P–Sn *peri* distances.

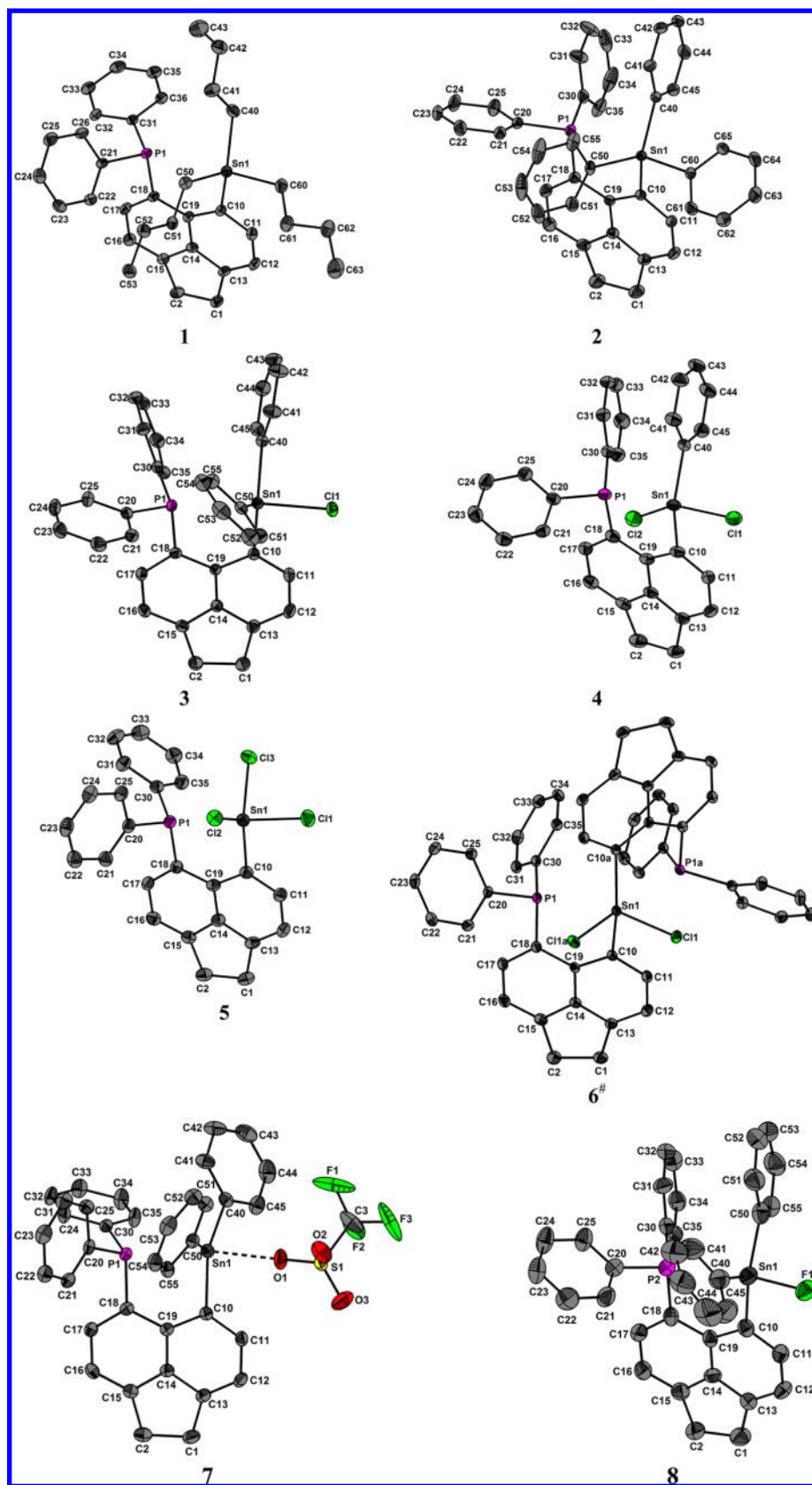


Figure 1. Molecular structures of 1–8 showing 30% probability ellipsoids and the crystallographic numbering scheme. (#) Symmetry code used to generate equivalent atoms for 6: (a) $1 - x, y, 1.5 - z$.

The smallest J values were observed for the tetraorganostannanes ArSnBu_3 (1; 202 Hz) and ArSnPh_3 (2; 284 Hz), having the longest P–Sn *peri* distances (3.332(2) and 3.2437(2) Å,

respectively). The largest J values were found for the diaryl tin dichlorides ArPhSnCl_2 (4; 906 Hz) and Ar_2SnCl_2 (6; 1011 Hz), comprising P–Sn *peri* distances (2.855(2) and 2.918(2)

Table 1. Experimental Bond Distances (Å) and Angles (deg) of 1–8

	1 ^a	2 ^a	3 ^b	4 ^c	5 ^d	6 ^e	7 ^f	8 ^g
Sn1–C10	2.191(4)	2.156(2)	2.161(2)	2.158(4)	2.130(4)	2.144(3)	2.145(3)	2.161(8)
Sn1–X	2.166(5)	2.142(2)	2.4913(6)	2.451(1)	2.399(1)	2.442(1)	2.391(3)	2.005(6)
Sn1–Y	2.158(5)	2.146(2)	2.142(2)	2.366(1)	2.362(1)		2.123(3)	2.126(12)
Sn1–Z	2.180(5)	2.167(2)	2.137(2)	2.127(4)	2.351(1)		2.128(3)	2.165(11)
C10–Sn1–X	121.2(2)	113.42(8)	123.15(8)	97.9(1)	99.2(1)	100.52(8)	89.7(1)	93.1(3)
C10–Sn1–Y	111.9(2)	106.75(9)	122.74(7)	113.9(1)	124.8(1)	152.5(2)	120.0(1)	120.8(4)
C10–Sn1–Z	104.0(2)	106.11(8)	95.83(5)	130.3(2)	122.0(1)		119.4(1)	121.5(4)
X–Sn1–Y	110.9(2)	120.48(9)	93.49(6)	93.80(5)	91.91(5)	98.87(8)	86.8(1)	96.1(4)
X–Sn1–Z	101.1(2)	102.57(8)	94.21(6)	95.5(1)	93.32(6)	89.64(6)	91.4(1)	98.5(3)
Y–Sn1–Z	105.8(2)	106.34(8)	112.23(8)	112.7(1)	110.94(5)		120.6(1)	114.6(4)

^aX = C40, Y = C50, Z = C60. ^bX = Cl1, Y = C40, Z = C50. ^cX = Cl1, Y = Cl2, Z = C40. ^dX = Cl1, Y = Cl2, Z = Cl3. ^eX = Cl1, Y = C10a, Z = Cl1a. Symmetry code used to generate equivalent atoms: (a) 1 – x, y, 1.5 – z. ^fX = O1, Y = C40, Z = C50. ^gX = F1, Y = C40, Z = C50.

Å) in the midrange. The aryltin trichloride ArSnCl₃ (**5**), revealing the shortest P–Sn *peri* distance (2.757(2) Å), gives rise to a comparatively small *J* value (635 Hz) which is comparable with that of the triaryltin chloride ArPh₂SnCl (**3**; 622 Hz). In addition to the dependence on the P–Sn distances the *J*(¹¹⁹Sn–³¹P) coupling constants might be also affected by the “re-hybridization” upon going from a tetrahedral to a trigonal-bipyramidal arrangement and the depleting *s* character of the Sn orbitals involved in the interaction with the lone pair of the P atom. In a tetrahedral arrangement, this Sn orbital is of the sp³ type, whereas in the case of three-center–four-electron (3c-4e) axial bonding of the trigonal bipyramid, the p_z orbital of the Sn atom is involved.¹⁴ Since the magnitude of *J* couplings correlates with the *s* character of the orbitals, the “re-hybridization” will adversely affect the shortening of the P–Sn *peri* distance. Inspection of the geometrical goodness of the five distorted-trigonal-bipyramidal structures suggests that ArSnPhCl₂ (**4**; ΔΣ(*θ*) = 69.7°) has a higher *s* character than ArSnPh₂Cl (**3**; ΔΣ(*θ*) = 74.6°) and ArSnCl₃ (**5**; ΔΣ(*θ*) = 73.3°), which might explain the large *J* value.

Despite ArPh₂SnO₃SCF₃ (**7**) showing the shortest P–Sn *peri* distance, the *J*-value is only in the midrange because the nearly perfect trigonal-bipyramidal structure (ΔΣ(*θ*) = 92.1°) reduces the *s* character to a minimum. The geometrical goodness values of ArSnPh₂F (**8**; ΔΣ(*θ*) = 69.2°) and ArSnPhCl₂ (**4**; ΔΣ(*θ*) = 69.7°) are very similar, but the different P–Sn *peri* distances (2.937(3) and 2.855(2) Å) might be the reason for the fact that the *J* value of **8** is smaller than that of **4**. The ¹⁹F NMR signal (CD₂Cl₂) of the triaryltin fluoride **8** shows a doublet centered at δ –184.9 (*J*(³¹P–¹⁹F) 84 Hz) with tin satellites (¹*J*(¹¹⁹Sn–¹⁹F) 2232 Hz), which compares reasonably well with that of the monomeric (Me₃SiCH₂)₃SnF (δ –207.2, ¹*J*(¹¹⁹Sn–¹⁹F) = 2370 Hz).³⁴

Gas-Phase and Electronic Structures. Gas-phase structures of **2–5**, **8**, the unsolvated triarylstannyl cation ArPh₂Sn⁺ (**7a**), and solvated triarylstannyl cation (ArPh₂Sn–NCMe)⁺ (**7b**) were obtained by geometry optimization at the B3PW91/6-311+G(2df,p) level of theory.³⁵ All gas-phase structures agree well with the corresponding solid-state structures; however, the Sn–P *peri* distances are about 0.1–0.15 Å longer. Nevertheless, all experimentally observed trends are fully retained. Parts a and b of Figure 2 show superpositions of the gas-phase structures of **2–5**, which reveal that mainly the Sn moiety accommodates the increasing strain on going from **5** to **2** in that only this fragment increases both its in-plane and out-of-plane distortions. This was also found for Br atoms in a series of 1-Br-8-[Ph₂P(E)]-Nap and 5-Br-6-[Ph₂P(E)]-Ace (E

= none, CH₃⁺, O, S, Se) compounds.³⁶ The rather large Sn atoms possess diffuse outer valence electrons and quite flexible Sn–C and Sn–Cl bonds in comparison to the rather rigid P–C bonds. As for the solid-state structures, the largest geometrical changes are found on going from **2** to **3**, which is due to the crucial electronic and steric influence of the substituent in the axial position.

In order to highlight the important role of the axial substituent, parts c and d of Figure 2 show the corresponding superpositions for the gas-phase structures of **3**, **7a,b** and **8**, comprising the axial substituents Cl (**3**), none (**7a**), MeCN (**7b**), and F (**8**). As expected, the charged species **7a,b** have the shortest Sn–P *peri* distances of 2.596 and 2.665 Å, respectively, which are very much like the corresponding distance in 5-(2',4',6'-*i*-Pr₃C₆H₂Sn)-6-(*i*-Pr₂P)-Ace (2.6362(6) Å).³⁰ However, at 3.038 and 3.045 Å the differences between **3** and **8** are rather marginal. The phenyl rings attached to the Sn atoms accommodate the steric stress by changing their orientation, whereas the orientation of the phenyl rings attached to the P atom remains almost unchanged in all considered compounds, which supports the idea that the Sn moiety is much more flexible than the P moiety. The complementary analysis of a set of topological and integrated real-space bonding indicators allows the determination of the characteristics of the Sn–P *peri* interaction. The topological bond paths motifs of **2**, **5**, and **7a,b** are displayed in Figure 3. Table 3 gives bond topological properties derived from AIM space partitioning, a set of ELI-D derived properties, and AIM charges of atoms and functional groups. In all compounds a Sn–P bond critical point (bcp) is detected which shows the typical characteristics of strongly polar (mainly ionic) bonded atoms,¹⁸ such as a very small value of the ED at the bcp (0.12 e Å⁻³ (**2**) to 0.46 e Å⁻³ (**7b**)), a positive Laplacian (but close to 0), a positive kinetic energy density to ρ(*r*)_{bcp} ratio (*G*/ρ(*r*)_{bcp}), and a total energy density to ρ(*r*)_{bcp} ratio (*H*/ρ(*r*)_{bcp}) that is negative but close to 0. Although it is weak, the Sn–P bond path in the electron density is stable in all gas-phase models, as the corresponding critical point is also found by subsequent analysis of the corresponding potential energy density (virial field, not shown). Note that the relative positions of the bcp are almost constant in this series (*d*₁/*d* = 47.3% (**2**) to 46.2% (**5**)). As expected, the bond parameters of **7a,b** extend the trend, which is generated by the series **2–5**, as a formal RPh₂Sn⁺ cation is a natural extension of a strongly polarized RPh₂SmO₃SCF₃ (**7**) moiety. As a result, the Sn–P interaction in **2** has to be considered as weakly ionic, whereas it is of polar-covalent nature in **7a,b**. In general, the ELI-D confirms the AIM results with one exception: for **2** a so-

Table 2. Experimental and Calculated (in Italics) Interatomic Distances (Å) and Angles (deg) of 1–8

	1	2	3	4
		<i>peri</i> Region Distances		
P(1)⋯Sn(1)	3.332(2)	3.247(2) 3.310	2.9075(6) 3.038	2.855(2) 2.990
		<i>peri</i> Region Bond Angles		
Sn(1)–C(10)–C(19)	129.6(3)	127.3(2) 128.90	122.3(2) 124.84	121.2(3) 123.74
C(10)–C(19)–C(18)	128.8(4)	128.3(2) 129.00	127.9(2) 128.42	127.9(4) 128.45
P(1)–C(18)–C(19)	120.6(3)	119.8(3) 120.21	117.8(2) 118.71	118.1(3) 118.14
∑ of bay angles	379(1)	375.4(7) 378.11	368.0(6) 371.97	367(1) 370.33
splay angle	19	15.4 18.11	8 11.97	7 10.33
C(20)–P(1)–C(30)	104.1(2)	102.0(2) 102.78	106.19(9) 104.33	105.8(2) 104.33
		Out-of-Plane Displacement		
P(1)	0.197(2) 0.243	0.3322(6) 0.128	0.0950(5) 0.178	0.083(2) ^a 0.129
Sn(1)	0.2529(6) 0.400	0.4284(3) 0.203	0.2503(2) 0.282	0.1691(3) ^a 0.227
		Central Acenaphthene Ring Torsion Angles		
C(13)–C(14)–C(19)–C(18)	179.6(5)	–179.5(3) 177.11	179.6(2) 178.65	–179.7(5) 177.78
C(15)–C(14)–C(19)–C(10)	177.9(4)	173.8(3) 176.04	177.3(3) 177.17	–179.9(4) 177.05
	5	6	7	8
		<i>peri</i> Region Distances		
P(1)⋯Sn(1)	2.757(2) 2.887	2.918(2)	2.7032(9) 2.665 ^b	2.937(3) 3.045
		<i>peri</i> Region Bond Angles		
Sn(1)–C(10)–C(19)	119.6(3) 122.01	122.9(2)	117.4(2) 116.79	123.7(6) 125.82
C(10)–C(19)–C(18)	128.2(3) 128.27	127.7(3)	128.4(3) 127.64	128.0(8) 128.06
P(1)–C(18)–C(19)	116.9(3) 117.64	115.5(2)	117.1(2) 117.52	117.3(6) 118.35
∑ of bay angles	364.7(9) 367.92	366.1(7)	362.9(7) 361.95	369(2) 372.23
splay angle	4.7 7.92	6.1	2.9 8.34	9 8.65
C(20)–P(1)–C(30)	107.0(2) 104.93	104.4(2) 105.65	109.1(2) 107.76	105.7(4) 104.44
		Out-of-Plane Displacement		
Sn(1)	0.0038(5) 0.237	0.4499(4)	0.0404(2) 0.213	0.1515(6) ^a 0.235
P(1)	0.008(2) 0.129	0.3279(8)	0.1990(8) 0.141	0.108(3) ^a 0.140
		Central Acenaphthene Ring Torsion Angles		
C(13)–C(14)–C(19)–C(18)	178.3(4) 178.49	172.4(3)	179.2(3) 178.06	–180.0(8) 178.01
C(15)–C(14)–C(19)–C(10)	–179.5(4) 177.65	178.0(3)	178.7(4) 178.11	178.2(8) 178.05

^aCompounds 4 and 7 have a cisoid out-of-plane displacement, and 1–3, 5, 6, and 8 show a transoid out-of-plane displacement. ^bCalculated interatomic distances and angles of 7b.

called monosynaptic valence basin ($V_1(P)$, that is a lone pair) is observed at the P atom instead of the expected disynaptic Sn–P basin ($V_2(Sn,P)$) that is found for 3–5 and 7a,b. An isosurface representation of the ELI-D of 2, 5, and 7a,b is given in Figure

4. Since the Sn–P distances of the optimized gas-phase geometries are 0.10–0.15 Å longer than those obtained by X-ray crystallography, the RSBI analysis is extended to the solid-state geometry of 2. However, all qualitative and quantitative

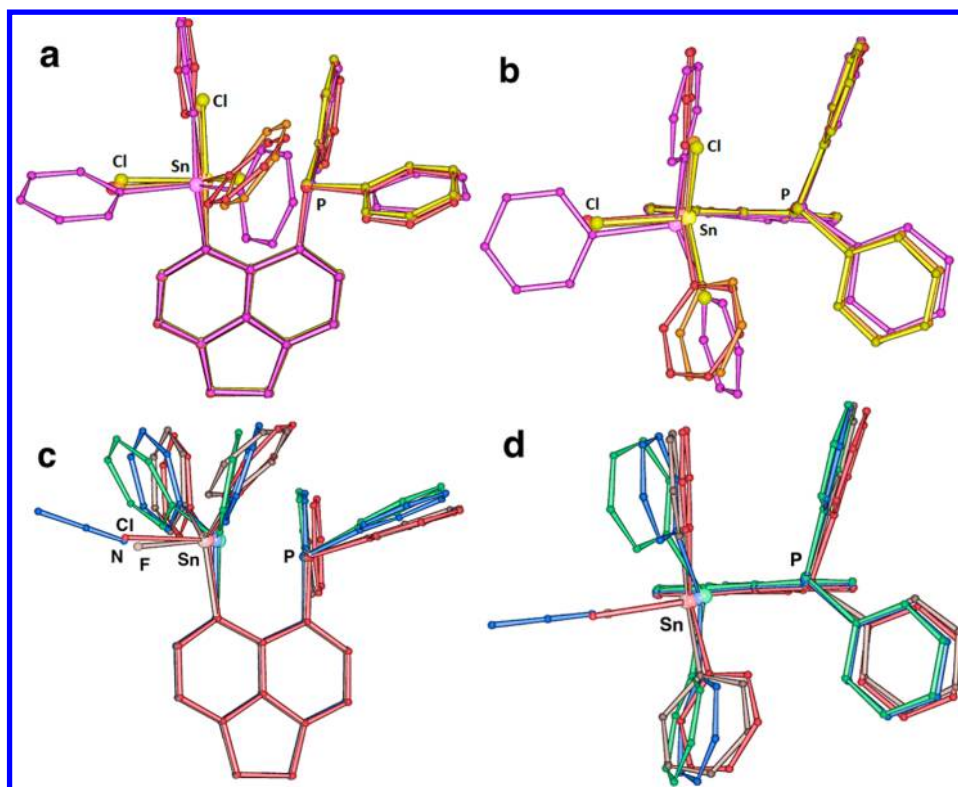


Figure 2. Superposition of the gas-phase structures of (a, b) 2 (violet), 3 (red), 4 (orange), and 5 (yellow) and (c, d) corresponding results for 3 (red), 7a (green), 7b (blue), and 8 (brown): (left) side-on view; (right) top view. All structures are SCHAKAL representations.³⁷

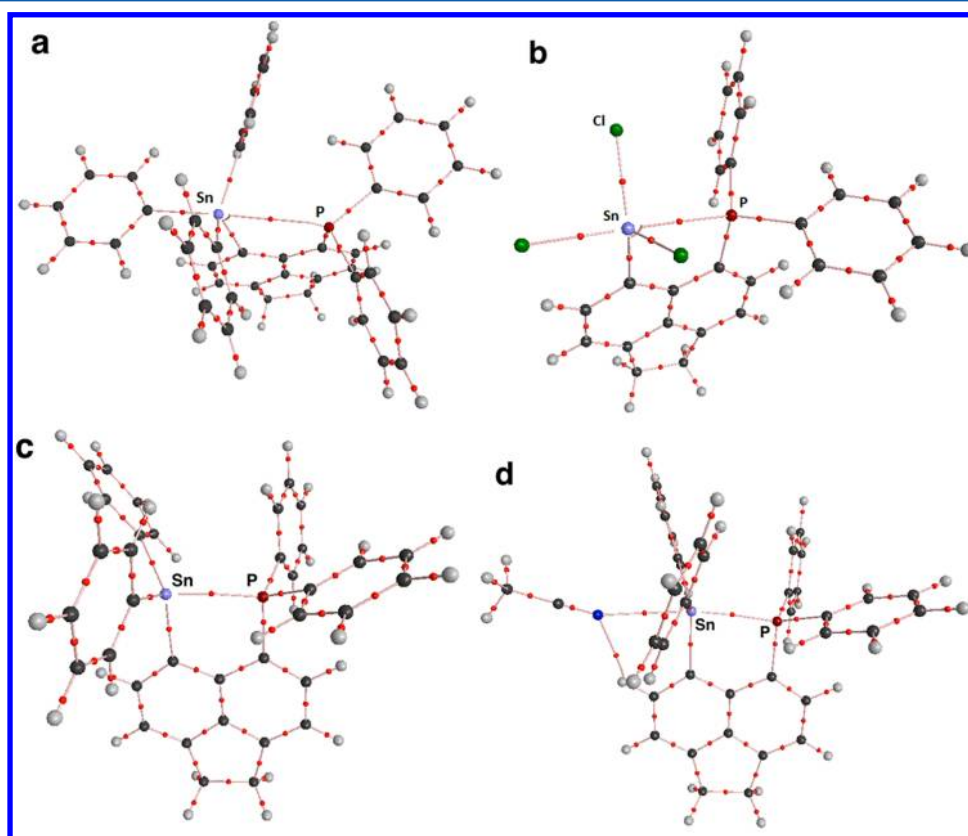


Figure 3. AIM bond paths of 2, 5, and 7a,b. Bond critical points are given as red dots. All structures are AIM2000 representations.³⁸

results between gas-phase and solid-state geometries of 2 are similar; hence, the topological difference between 2 and the

other compounds is not an artifact of the calculation. Interestingly, the different kinds of ligands attached to the Sn

Table 3. Topological and Integrated AIM and ELI-D Properties of 2–5, 7a,b, and 8^a

	Sn–P										
	d (Å)	$\rho(\mathbf{r})_{\text{bcp}}$ (e Å ⁻³)	$\nabla^2\rho(\mathbf{r})_{\text{bcp}}$ (e Å ⁻⁵)	d_1/d (%)	$G/\rho(\mathbf{r})_{\text{bcp}}$ (he ⁻¹)	$H/\rho(\mathbf{r})_{\text{bcp}}$ (he ⁻¹)	$N_{(001)}^{\text{ELI}}$ (e)	$V_{(001)}^{\text{ELI}}$ (Å ³)	Y_{max}	Δ_{ELI} (Å)	RJI (%)
2	3.310	0.12	0.7	47.3	0.45	−0.04	2.06	13.4	2.43		99
2exp	3.247	0.13	0.8	47.2	0.47	−0.05	2.06	12.6	2.41		98
3	3.038	0.19	0.8	46.4	0.44	−0.14	2.04	11.7	2.31	0.432	96
4	2.990	0.22	0.8	46.4	0.42	−0.17	2.05	11.6	2.29	0.397	94
5	2.887	0.27	0.7	46.2	0.41	−0.22	2.07	11.3	2.23	0.344	89
7a	2.596	0.46	0.8	46.6	0.46	−0.34	2.05	10.6	2.03	0.258	79
7b	2.665	0.41	0.9	46.3	0.46	−0.31	2.05	10.8	2.10	0.281	84
8	3.045	0.19	0.8	46.5	0.43	−0.14	2.04	12.1	2.33	0.458	95
	$Q_{\text{tot}}^{\text{AIM}}$ (e)										
	Ace	P	PPh ₂	Sn	X _{ax}	Cl _{eq}	Ph _{ax}	Ph _{eq}	SnX _n Ph _{3−n}		
2	−0.89	1.48	0.50	1.61			−0.44	−0.40, −0.42	0.35		
2exp	−0.90	1.50	0.50	1.63			−0.43	−0.40, −0.40	0.40		
3	−0.83	1.52	0.58	1.66	−0.66			−0.36, −0.36	0.28		
4	−0.81	1.52	0.60	1.76	−0.61	−0.61		−0.32	0.22		
5	−0.74	1.53	0.60	1.85	−0.59	−0.57, −0.56			0.13		
7a	−0.72	1.58	0.82	1.48				−0.30, −0.27	0.91		
7b	−0.74	1.53	0.73	1.58	0.03			−0.30, −0.31	1.00		
8	−0.83	1.49	0.55	1.79	−0.77			−0.37, −0.37	0.28		

^aFor all bonds, $\rho(\mathbf{r})_{\text{bcp}}$ is the electron density at the bond critical point, $\nabla^2\rho(\mathbf{r})_{\text{bcp}}$ is the corresponding Laplacian, d_1 and d_2 are the distances from the atom to the bond critical point, ε is the bond ellipticity ($\varepsilon = \lambda_1/\lambda_2 - 1$, where λ_1 and λ_2 are curvatures perpendicular to the bond path), λ_3 is the curvature along the bond path, and $G/\rho(\mathbf{r})_{\text{bcp}}$ and $H/\rho(\mathbf{r})_{\text{bcp}}$ are the ratios of kinetic and total energy density to $\rho(\mathbf{r})_{\text{bcp}}$. For all basins, $V_{(001)}^{\text{ELI}}$ is the basin volume cut at 0.001 au, $N_{(001)}^{\text{ELI}}$ is the corresponding electron population in that volume, Y_{max} is the ELI-D value at the attractor position, Δ_{ELI} is the perpendicular distance of the attractor position to the atom–atom line, and RJI is the Raub–Jansen index (percentile electron population within the AIM atom which has the larger electronegativity). Results were obtained by an analysis of the wave function files with AIM2000.³⁶

atom have only a small effect on the corresponding $V_2(\text{Sn,P})/V_1(\text{P})$ basin electron populations (2.04–2.07 e) and volumes (11.3–13.4 Å³), also in the case of the triarylstannyl cations **7a,b** (2.05 e, 10.6/10.8 Å³). Some trends, however, are visible for the topological ELI-D properties, such as the ELI-D value at the basin attractor position (Y_{max}), which is an indicator of the degree of electron delocalization, and the distance of this attractor to the Sn–P axis (Δ_{ELI}). Large Δ_{ELI} values are a sign for bond strain in covalent bonds and are typical for nondirected ionic bonds in solids. Both decrease in the order **2** > **8** > **3** > **4** > **5** > **7b** > **7a**. With increasing strength of the Sn–P interaction the electron localizability within the $V_2(\text{Sn,P})/V_1(\text{P})$ basin decreases as electrons are shared. The Δ_{ELI} values are generally quite large, which may indicate some strain in the Sn–P interactions. Since the Sn–P *peri* interaction is established by the lone pair of the PPh₂ fragment, which is in accordance with the observation that the $V_2(\text{Sn,P})/V_1(\text{P})$ basin is located much closer to the P atom (see Figure 4), the RJI helps to understand how much this “lone pair” is involved in the interaction. As expected, the RJI is found to be 99% for **2**, which means that 99% of the ED of the $V_2(\text{Sn,P})$ basin remains in the AIM atomic basin of the P atom and is consistent with an almost nonbonding scenario. For **5** and **7a,b** the RJI values are 89%, 79%, and 84%, respectively, which are in the range of polar-covalent interactions. **3**, **4**, and **8** are intermediate cases. The recently introduced mapping of the ELI-D distribution on the surface of an ELI-D basin⁴⁰ is a suitable tool to uncover weak effects of electron redistribution due to chemical bonding and has been applied to related *peri*-substituted (ace)-naphthylphosphinoboranes **IV** and **V** before (Scheme 1).⁶ Figure 5 shows the ELI-D distribution mapped on the $V_1(\text{P})$ basin in **2** and the $V_2(\text{Sn,P})$ basins in **5** and **7a,b**. Disregarding the fact that for **2** the lone pair basin of the P atom is flattened

in the P–Sn direction and is not connected to the Sn atom in terms of the ELI-D topology, a region of slightly increased electron localizability directed toward the Sn atom is already visible. This effect is significantly enhanced for the bonding interactions in **5** and **7a,b**. Thus, it can be stated that the Sn–P contact in **2** is in a border regime between nonbonding and weakly ionic. On the one hand, the relevant basin is assigned as a P atom lone pair basin and the electrons of this basin remain at 99% in the AIM P atom. On the other hand, a region of increased localizability is visible in the Sn direction on the basin surface and, moreover, a bcp is found in the underlying ED and virial field. With increased Lewis acidity of the Sn atom the Sn–P bonding becomes a strongly polar covalent interaction with considerable covalent contributions for **5**, **7b**, and **7a**, which is reflected in the decreased Y_{max} , Δ_{ELI} , $H/\rho(\mathbf{r})_{\text{bcp}}$, and RJI values and increased $\rho(\mathbf{r})_{\text{bcp}}$ values. The AIM and ELI-D properties of the P–C and Sn–C bonds are similar to those found in previous studies.^{6,36,42} Consequently, it may be stated that these bonds are only slightly affected by the (non)bonding *peri* interaction. An exception is the RJI, for which considerable changes are observed (73–78% for P–C, 68–77% for Sn–C). These results prove the essential contributions of the combined AIM and ELI-D bond analysis. AIM charges of all relevant atoms and functional groups of **2–5** and **7a,b** are shown in Table 3. Going from **2** to **5**, the redistribution of electrons as a consequence of the introduction of Cl atoms becomes visible and these effects are obviously far reaching, as all fragments are influenced by the number of Cl atoms. The acenaphthene ring system and the P atom each lose 0.15 e in this series, whereas the Sn atom, which is directly bonded to the Cl atom(s), loses 0.24 e. In addition, the Cl atom AIM charges become less negative with an increasing number of competing Cl atoms. For comparison, Sn AIM atomic charges have also been determined

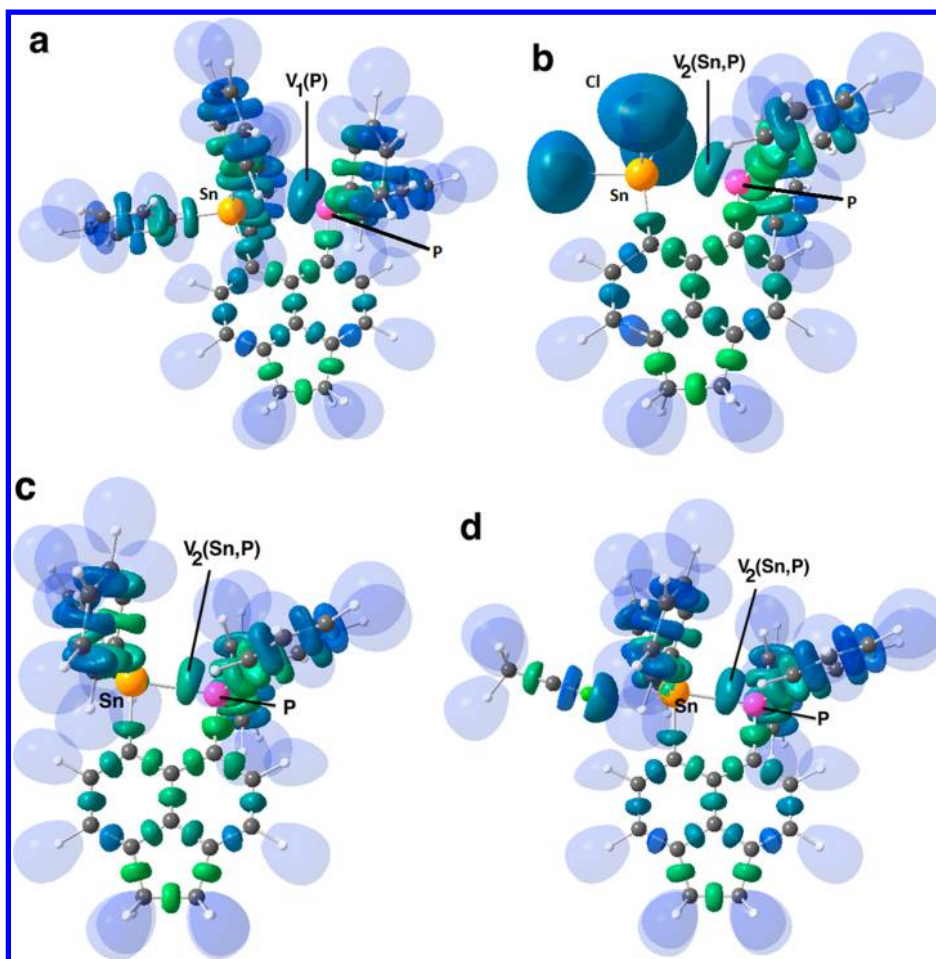


Figure 4. Isosurface representations of the localization domains of the ELI-D ($Y = 1.4$) of **2**, **5**, and **7a,b**. The color is coded according to the corresponding basin volumes transforming from green (small) to blue (large). For clarity, the protonated valence basins (H atoms) are given in transparent mode.

for the optimized gas-phase models of Ph_3Sn^+ and Ph_3SnCl , being 1.53 and 1.68 e, respectively. The former lies between the results for **7a** (1.48 e) and **7b** (1.58 e), whereas the latter compares well with the result for **3** (1.66 e). As expected, the positive molecular charges in **7a,b** mainly affect the $\text{SnPh}_{2-n}\text{X}_n$ part of the molecule. Nevertheless, the AIM charges of the Sn atom are significantly less positive in **7a,b** in comparison to all others because of the lack of a third substituent with electron-withdrawing properties. At 1.48 e, the Sn AIM atomic charge of **7a** is even less positive than the charge of the P atom in **7a** (1.58 e). Accordingly, **7a** may be regarded as a stannyl-substituted phosphonium ion rather than a phosphine-supported triarylstannyl cation.⁴⁴

CONCLUSIONS

The series of (6-(diphenylphosphino)acenaphth-5-yl)stannanes ArSnBu_3 (**1**), ArSnPh_3 (**2**), ArSnPh_2Cl (**3**), ArSnPhCl_2 (**4**), ArSnCl_3 (**5**), Ar_2SnCl_2 (**6**), $\text{ArSnPh}_2\text{O}_3\text{SCF}_3$ (**7**), and ArSnPh_2F (**8**), containing intramolecularly coordinated P donor substituents, was prepared and fully characterized (Ar = 6- $\text{Ph}_2\text{P-Ace-5-}$). While hypercoordinated organostannanes containing N and O donor substituents have been extensively investigated,^{8,10,11} P donor substituents are much rarer.⁴⁵ Inspection of the molecular geometries revealed that the more flexible $\text{SnPh}_{3-n}\text{X}_n$ part of the molecule accommodates the steric strain due to the *peri* interaction, whereas the

orientation of the more rigid PPh_2 part remains almost unchanged. The Lewis acidity of the Sn atom can be fine-tuned by the choice of the substituents attached to the Sn atom; especially the axial substituent (X) has a crucial role due to the possible formation of 3c-4e P–Sn–X bonds. Analysis of a set of RSBI values derived from the electron and pair densities of the gas-phase structures showed the Sn–P *peri* interaction in **2** to be in the border regime between nonbonding and weakly ionic bonding. In the order $8 < 3 < 4 < 5 < 7b < 7a$ the Sn–P interaction becomes a polar-covalent interaction with a considerable degree of covalency. We are currently using **1** as the starting material in transmetalation reactions for the synthesis of new *peri*-substituted acenaphthyl compounds containing elements such as Hg, Au, B, Ga, In, As, Sb, and Te.

EXPERIMENTAL SECTION

General Considerations. Reagents were obtained commercially and used as received (Sigma-Adrich, Germany). 5-Bromo-6-(diphenylphosphino)acenaphthene was prepared according to literature procedures.³⁶ Dry solvents were collected from a SPS800 mBraun solvent system. ^1H , ^{13}C , ^{19}F , ^{31}P , and ^{119}Sn NMR spectra were recorded at room temperature using a Bruker Avance-360 spectrometer and are referenced to tetramethylsilane (^1H , ^{13}C), trichlorofluoromethane (^{19}F), phosphoric acid (85% in water; ^{31}P), and tetramethyltin (^{119}Sn). Chemical shifts are reported in parts per million (ppm), and coupling constants (J) are given in hertz (Hz). Electron impact mass spectroscopy (EIMS) was carried out using a

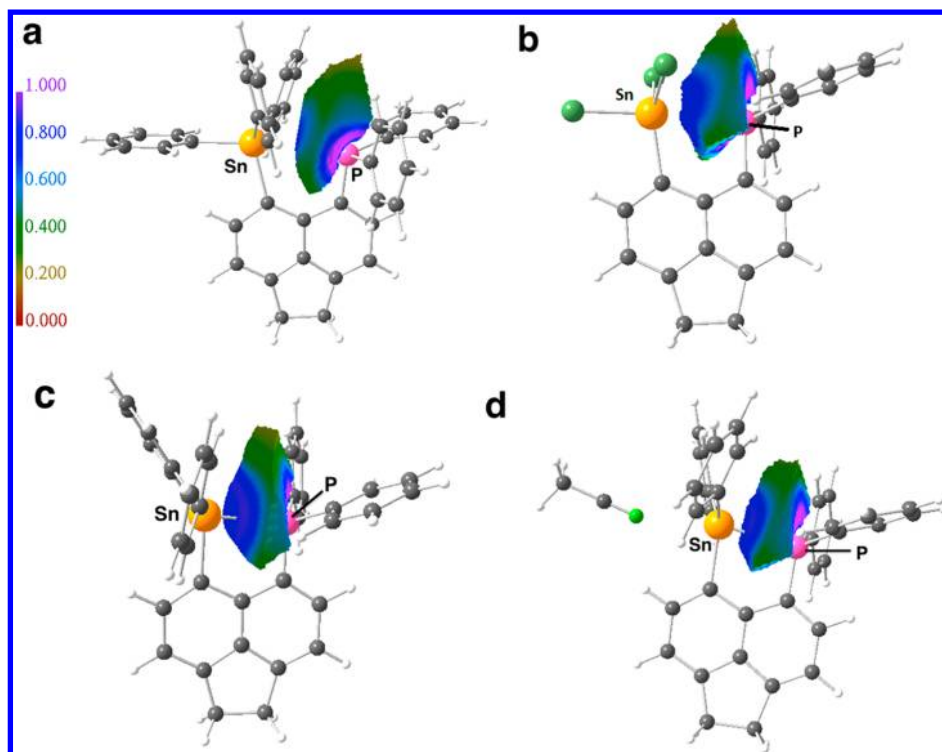


Figure 5. ELD distribution mapped on (a) the P lone pair basin ($V_1(P)$) of **2** and (b–d) the Sn–P basins ($V_2(\text{Sn},P)$) of (b) **5**, (c) **7a**, and (d) **7b**. All structures are MOLISO representations.⁴¹

Finnigan MAT 95 instrument. The ESI MS spectra were obtained with a Bruker Esquire-LC MS instrument. Dichloromethane/acetonitrile solutions (or otherwise stated, $c = 1 \times 10^{-6}$ mol L⁻¹) were injected directly into the spectrometer at a flow rate of 3 $\mu\text{L min}^{-1}$.

Nitrogen was used both as a drying gas and for nebulization with flow rates of approximately 5 L min⁻¹ and a pressure of 5 psi, respectively. Pressure in the mass analyzer region was usually about 1×10^{-5} mbar. Spectra were collected for 1 min and averaged.

The nozzle-skimmer voltage was adjusted individually for each measurement. The conductivity measurement of [5-(Ph₂Sn-6-(Ph₂P)-Ace)]O₃SCF₃ (**7**) was carried out with a WTW Cond 330i instrument at 298 K.

Synthesis of (6-(Diphenylphosphino)acenaphth-5-yl)-tributyltin (1). *n*-Butyllithium (43.1 mmol, 2.5 M in *n*-hexane) and *N,N,N',N'*-tetramethylethylenediamine (5.01 g, 43.1 mmol) were added at -78°C to a suspension of 5-bromo-6-(diphenylphosphino)acenaphthene (15.0 g, 36.0 mmol) in diethyl ether (180 mL), and the mixture was stirred for 2 h at this temperature. The suspension was warmed to room temperature and stirred for 1 h, tributyltin chloride (14.0 g, 43.1 mmol) was added dropwise, and stirring was continued for 12 h. After aqueous workup the removal of the solvent by rotary evaporation afforded a brownish oil which solidified upon standing. The solid was washed intensely with acetonitrile and dried under vacuum, affording **1** as a colorless solid (16.1 g, 25.7 mmol, 71%; mp 54°C). Crystals suitable for X-ray crystallography were obtained by recrystallization from toluene at 5°C .

¹H NMR (CDCl₃): δ 7.89 (d, ³J(¹H–¹H) = 7 Hz, ³J(^{119/117}Sn–¹H) = 52/50 Hz, 1H, H-4), 7.49–7.29 (m, 13H), 3.49–3.47 (m, 4H, H-1,2), 1.65–1.57 (m, 6H, CH₂- β), 1.40–1.32 (m, 6H, CH₂- γ), 1.30–1.25 (m, 6H, CH₂- α), 0.93 ppm (t, ³J(¹H–¹H) = 7.3 Hz, 9H, CH₃). ¹³C{¹H} NMR (CDCl₃): δ 149.8 (s, C_b or C_c), 147.0 (d, J(³¹P–¹³C) = 2 Hz, C_c or C_b), 142.3 (d, J(³¹P–¹³C) = 29 Hz, C₆ or C_{i,P-phenyl}), 139.7 (d, ²J(³¹P–¹³C) = 7 Hz, C_a or C₇), 139.3 (d, ⁴J(³¹P–¹³C) = 2 Hz, ²J(^{119/117}Sn–¹³C) = 35 Hz, C₄), 138.2 (d, ³J(³¹P–¹³C) = 10 Hz, C₅), 137.9 (d, ⁴J(³¹P–¹³C) = 2 Hz, C_d), 135.1 (d, J(³¹P–¹³C) = 26 Hz, C_{i,P-phenyl} or C₆), 132.9 (d, ²J(³¹P–¹³C) = 17 Hz, C_{o,P-phenyl}), 129.8 (d, ²J(³¹P–¹³C) = 9 Hz, C₇ or C_a), 128.3 (d, ³J(³¹P–¹³C) = 6 Hz, C_{m,P-phenyl}), 128.0 (s, C_{p,P-phenyl}), 119.7 (s, ³J(^{119/117}Sn–¹³C) = 47 Hz,

C₃), 119.5 (s, C₈), 30.0 (s, C₁ or C₂), 29.9 (s, C₂ or C₁), 29.3 (d, J(³¹P–¹³C) = 2 Hz, ²J(^{119/117}Sn–¹³C) = 19 Hz, C₆), 27.5 (s, ³J(^{119/117}Sn–¹³C) = 68/62 Hz, C₇), 14.3 (d, J(³¹P–¹³C) = 21 Hz, ¹J(^{119/117}Sn–¹³C) = 362/346 Hz, C_a), 13.7 ppm (s, CH₃). ³¹P{¹H} NMR (CDCl₃): δ –25.9 ppm (s, J(^{119/117}Sn–³¹P) = 202/193 Hz). ¹¹⁹Sn{¹H} NMR (CDCl₃): δ –55.7 ppm (d, J(³¹P–¹¹⁹Sn) = 202 Hz). MS (EI⁺): m/z 571 [M – C₄H₉]⁺.

Synthesis of (6-(Diphenylphosphino)acenaphth-5-yl)-triphenyltin (2). To a suspension of 5-bromo-6-(diphenylphosphino)acenaphthene (1.00 g, 2.40 mmol) in diethyl ether (10 mL) were added *n*-butyllithium (2.88 mmol, 2.5 M in *n*-hexane) and *N,N,N',N'*-tetramethylethylenediamine (0.33 g, 2.88 mmol) at -78°C . After 2 h the suspension was warmed to room temperature and stirred for 1 h, triphenyltin chloride (1.11 g, 2.88 mmol) was added, and stirring was continued for 12 h. Dichloromethane was added to the suspension, and after aqueous workup the removal of the solvent by rotary evaporation afforded a white solid, which was recrystallized from dichloromethane and *n*-hexane, affording **2** as colorless crystals (1.22 g, 1.77 mmol, 74%; mp 223°C).

¹H NMR (CDCl₃): δ 7.95 (d, ³J(¹H–¹H) = 7 Hz, ³J(^{119/117}Sn–¹H) = 67/64 Hz, 1H, H-4), 7.69 (dd, ³J(¹H–¹H) = 8 Hz, ⁴J(¹H–¹H) = 2 Hz, ³J(^{119/117}Sn–¹H) = 48 Hz, 6H, H–C_{o,Sn-phenyl}), 7.45–7.28 (m, 12H), 7.22 (t, ³J(¹H–¹H) = 7 Hz, 2H), 7.09 (dt, ³J(¹H–¹H) = 8 Hz, ⁴J(¹H–¹H) = 2 Hz, 4H), 6.63 (t, ³J(¹H–¹H) = 8 Hz, 4H), 3.52 ppm (s, 4H, H-1,2). ¹³C{¹H} NMR (CDCl₃): δ 149.8 (s, J(^{119/117}Sn–¹³C) = 9 Hz, C_b or C_c), 148.5 (d, J(³¹P–¹³C) = 2 Hz, J(^{119/117}Sn–¹³C) = 12 Hz, C_c or C_b), 144.0 (d, ³J(³¹P–¹³C) = 21 Hz, ¹J(^{119/117}Sn–¹³C) = 561/536 Hz, C₃), 142.0 (d, ⁴J(³¹P–¹³C) = 2 Hz, ²J(^{119/117}Sn–¹³C) = 49 Hz, C₄), 142.0 (d, ¹J(³¹P–¹³C) = 29 Hz, C₆ or C_{i,P-phenyl}), 139.9 (d, ²J(³¹P–¹³C) = 7 Hz, C_a or C₇), 137.8 (d, J(³¹P–¹³C) = 2 Hz, C_{i,Sn-phenyl}), 137.0 (s, ²J(^{119/117}Sn–¹³C) = 35 Hz, C_{o,Sn-phenyl}), 136.7 (d, ⁴J(³¹P–¹³C) = 7 Hz, C_d), 132.8 (d, ²J(³¹P–¹³C) = 17 Hz, C_{o,P-phenyl}), 130.7 (d, ¹J(³¹P–¹³C) = 31 Hz, C_{i,P-phenyl} or C₆), 129.4 (d, ²J(³¹P–¹³C) = 7 Hz, C₇ or C_a), 128.2 (s, ³J(^{119/117}Sn–¹³C) = 51 Hz, C_{m,Sn-phenyl}), 127.8 (d, ³J(³¹P–¹³C) = 7 Hz, C_{m,P-phenyl}), 127.8 (s, C_{p,Sn-phenyl}), 127.6 (s, C_{p,P-phenyl}), 120.1 (d, ⁵J(³¹P–¹³C) = 1 Hz, ³J(^{119/117}Sn–¹³C) = 64 Hz, C₃), 119.9 (d, ³J(³¹P–¹³C) = 1 Hz, C₈), 30.1 (s, C₁ or C₂), 30.1

ppm (s, C₂ or C₁). ³¹P{¹H} NMR (CDCl₃): δ -30.6 ppm (s, J(^{119/117}Sn-³¹P) = 284/271 Hz). ¹¹⁹Sn{¹H} NMR (CDCl₃): δ -157.9 ppm (d, J(³¹P-¹¹⁹Sn) = 284 Hz). ESI MS (CH₂Cl₂/MeCN 1/10, positive mode): *m/z* 711.3 (NaC₄₂H₃₃PSn) for [5-(SnPhCl₂)-6-(Ph₂P)Ace + Na⁺].

Synthesis of (6-(Diphenylphosphino)acenaphth-5-yl)-diphenyltin Chloride (3). *Method a.* A solution of (6-(diphenylphosphino)acenaphth-5-yl)tributyltin (1; 250 mg, 0.40 mmol) in toluene (2 mL) was slowly added to a solution of diphenyltin dichloride (137 mg, 0.40 mmol) in 2 mL of toluene. The reaction mixture was stirred at 120 °C for 3 h, cooled to room temperature, and stirred for a further 12 h. The precipitate was filtered, washed three times with toluene, and dried under vacuum, affording 3 (40.2 mg, 0.06 mmol, 15%) as a white solid. Crystals suitable for X-ray were obtained by recrystallization from dichloromethane.

Method b. *n*-Butyllithium (1.20 mmol, 2.5 M in *n*-hexane) and *N,N,N',N'*-tetramethylethylenediamine (0.14 g, 1.20 mmol) were added at -78 °C to a suspension of 5-bromo-6-(diphenylphosphino)acenaphthene (0.50 g, 1.20 mmol) in diethyl ether (5 mL) and stirred for 2 h at this temperature. The suspension was warmed to room temperature and stirred for 1 h, diphenyltin dichloride (0.41 g, 1.20 mmol) was slowly added, and stirring was continued for 12 h. The precipitate was allowed to settle, the solution was decanted, and the solid was washed with diethyl ether. Dichloromethane (30 mL) was added to the solid, and after aqueous workup the removal of the solvent by rotary evaporation afforded a white solid. Recrystallization from dichloromethane and *n*-hexane yielded 3 as colorless crystals (272 mg, 0.42 mmol, 35%; mp 210 °C dec).

¹H NMR (CDCl₃): δ 8.98 (d, ³J(¹H-¹H) = 7 Hz, ³J(^{119/117}Sn-¹H) = 80/77 Hz, 1H, H-4), 7.67 (d, ³J(¹H-¹H) = 7 Hz, 1H), 7.61 (dd, ³J(¹H-¹H) = 8 Hz, ⁴J(¹H-¹H) = 1 Hz, ³J(^{119/117}Sn-¹H) = 67 Hz, 4H, H-C₆, Sn-phenyl), 7.46-7.37 (m, 2H), 7.26-7.15 (m, 8H), 7.07 (dt, ³J(¹H-¹H) = 8 Hz, ⁴J(¹H-¹H) = 2 Hz, 4H), 6.77 (dt, ³J(¹H-¹H) = 9 Hz, ⁴J(¹H-¹H) = 1 Hz, 4H), 3.57-3.51 ppm (m, 4H, H-1,2). ¹³C{¹H} NMR (CDCl₃): δ 151.3 (d, J(³¹P-¹³C) = 2 Hz, C_b or C_c), 149.1 (d, J(³¹P-¹³C) = 2 Hz, C_c or C_d), 142.3 (d, J(³¹P-¹³C) = 27 Hz, C_s, C₆ or C_{i,P}-phenyl), 141.4 (d, ⁴J(³¹P-¹³C) = 6 Hz, C₄), 139.8 (d, ²J(³¹P-¹³C) = 8 Hz, C_a or C₇), 137.1 (d, J(³¹P-¹³C) = 2 Hz, C_{i,Sn}-phenyl), 135.9 (d, J(³¹P-¹³C) = 2 Hz, ²J(^{119/117}Sn-¹³C) = 46 Hz, C_{o,Sn}-phenyl), 132.8 (d, ²J(³¹P-¹³C) = 13 Hz, C_{o,P}-phenyl), 131.5 (d, ²J(³¹P-¹³C) = 16 Hz, C₇ or C_a), 129.8 (d, J(³¹P-¹³C) = 44 Hz, C_s, C₆ or C_{i,P}-phenyl), 129.1 (d, ⁴J(³¹P-¹³C) = 1 Hz, C_{p,P}-phenyl), 128.7 (s, C_{p,Sn}-phenyl), 128.5 (s, ³J(^{119/117}Sn-¹³C) = 73/70 Hz, C_{m,Sn}-phenyl), 128.3 (d, ³J(³¹P-¹³C) = 9 Hz, C_{m,P}-phenyl), 124.5 (d, ¹J(³¹P-¹³C) = 18 Hz, C_s, C₆ or C_{i,P}-phenyl), 121.4 (d, ⁵J(³¹P-¹³C) = 3 Hz, C₃), 120.0 (d, ³J(³¹P-¹³C) = 4 Hz, C₈), 30.6 (s, C₁ or C₂), 30.2 ppm (s, C₂ or C₁). ³¹P{¹H} NMR (CDCl₃): δ -33.2 ppm (s, J(^{119/117}Sn-³¹P) = 628/601 Hz). ¹¹⁹Sn{¹H} NMR (CDCl₃): δ -200.8 ppm (d, J(³¹P-¹¹⁹Sn) = 622 Hz). ESI MS (CH₂Cl₂/MeOH 1/10, positive mode): *m/z* 611.3 (C₃₆H₂₈P₂Sn) for [5-(SnPh₂Cl)-6-(Ph₂P)Ace - Cl⁻].

Synthesis of (6-(Diphenylphosphino)acenaphth-5-yl)-phenyltin Dichloride (4). A solution of (6-(diphenylphosphino)acenaphth-5-yl)tributyltin (1; 2.50 g, 3.98 mmol) in *n*-hexane (20 mL) was slowly added to phenyltin trichloride (1.20 g, 3.98 mmol) and the reaction mixture was stirred at room temperature for 12 h. The precipitate was filtered, washed three times with *n*-hexane, and dried under vacuum, affording a white solid of 4 (2.05 g, 3.39 mmol, 85%, mp 217 °C). Crystals suitable for X-ray crystallography were obtained by recrystallization from dichloromethane and *n*-hexane.

¹H NMR (CDCl₃): δ 8.89 (d, ³J(¹H-¹H) = 7 Hz, ³J(^{119/117}Sn-¹³C) = 107/104 Hz, 1H, H-4), 7.65 (d, ³J(¹H-¹H) = 7 Hz, ³J(^{119/117}Sn-¹H) = 47 Hz, 2H, H-C₆, Sn-phenyl), 7.57 (t, ³J(¹H-¹H) = 7 Hz, 1H), 7.46-7.15 (m, 15H), 3.53 ppm (s, 4H, H-1,2). ¹³C{¹H} NMR (CDCl₃): δ 151.7 (d, J(³¹P-¹³C) = 2 Hz, C_b or C_c), 150.8 (d, J(³¹P-¹³C) = 2 Hz, C_c or C_d), 144.3 (d, J(³¹P-¹³C) = 42 Hz, C_s, C₆ or C_{i,P}-phenyl), 140.6 (d, ⁴J(³¹P-¹³C) = 8 Hz, C₄), 139.9 (d, J(³¹P-¹³C) = 22 Hz, C_a, C_d or C₇), 139.7 (d, J(³¹P-¹³C) = 7 Hz, C_a, C_d or C₇), 136.9 (d, J(³¹P-¹³C) = 2 Hz, C_{i,Sn}-phenyl), 134.0 (d, J(³¹P-¹³C) = 2 Hz, ²J(^{119/117}Sn-¹³C) = 62 Hz, C_{o,Sn}-phenyl), 133.1 (d, ²J(³¹P-¹³C) = 13 Hz,

C_{o,P}-phenyl), 129.9 (d, J(³¹P-¹³C) = 22 Hz, C_s, C₆ or C_{i,P}-phenyl), 129.9 (d, ⁴J(³¹P-¹³C) = 2 Hz, C_{p,P}-phenyl), 129.6 (s, C_{p,Sn}-phenyl), 128.8 (s, ³J(^{119/117}Sn-¹³C) = 99/95 Hz, C_{m,Sn}-phenyl), 128.6 (d, ³J(³¹P-¹³C) = 9 Hz, C_{m,P}-phenyl), 122.3 (d, ¹J(³¹P-¹³C) = 24 Hz, C_s, C₆ or C_{i,P}-phenyl), 121.3 (d, ⁵J(³¹P-¹³C) = 5 Hz, ³J(^{119/117}Sn-¹³C) = 102 Hz, C₃), 120.5 (d, ³J(³¹P-¹³C) = 5 Hz, C₈), 30.7 (s, C₁ or C₂), 30.3 ppm (s, C₂ or C₁). ³¹P{¹H} NMR (CDCl₃): δ -39.0 ppm (s, J(^{119/117}Sn-³¹P) = 906/866 Hz). ¹¹⁹Sn{¹H} NMR (CDCl₃): δ -202.5 ppm (d, J(³¹P-¹¹⁹Sn) = 904 Hz). ESI MS (CH₂Cl₂/MeCN 1/10, positive mode): *m/z* 596.2 (C₃₀H₂₃Cl₂PSn) for [5-(SnPhCl₂)-6-(Ph₂P)Ace - Cl⁻]. ESI MS (CH₂Cl₂/MeCN 1/10, negative mode): *m/z* 638.9 (C₃₀H₂₃Cl₃PSn) for [5-(SnPhCl₂)-6-(Ph₂P)Ace + Cl⁻].

Synthesis of (6-(Diphenylphosphino)acenaphth-5-yl)tin Trichloride (5). To a vigorously stirred solution of tin(IV) chloride (2.00 g, 7.68 mmol) in *n*-hexane (20 mL) was slowly added (6-(diphenylphosphino)acenaphth-5-yl)tributyltin (1; 2.50 g, 3.98 mmol), causing immediate precipitation of the crude product. Stirring was continued at room temperature for 12 h. The precipitate was filtered, washed three times with *n*-hexane, and dried under vacuum, affording 5 (2.16 g, 3.85 mmol, 97%, mp 153 °C dec) as a white solid. Crystals suitable for X-ray crystallography were obtained by recrystallization from toluene.

¹H NMR (CDCl₃): δ 8.64 (dd, ³J(¹H-¹H) = 7 Hz, ⁵J(³¹P-¹H) = 3 Hz, ³J(^{119/117}Sn-¹H) = 144 Hz, H1, H-4), 7.65 (t, ³J(¹H-¹H) = 8 Hz, 2H), 7.57-7.43 (m, 11H), 3.58 ppm (s, 4H, H-1,2). ¹³C{¹H} NMR (CDCl₃): δ 152.6 (d, J(³¹P-¹³C) = 2 Hz, C_b or C_c), 151.8 (d, J(³¹P-¹³C) = 2 Hz, C_c or C_d), 139.5 (d, ⁴J(³¹P-¹³C) = 10 Hz, C₄), 139.3 (s), 138.3 (d, ²J(³¹P-¹³C) = 17 Hz, C_a or C₇), 137.1 (d, ⁴J(³¹P-¹³C) = 2 Hz, C_d), 133.7 (d, ²J(³¹P-¹³C) = 12 Hz, C_{o,P}-phenyl), 131.1 (d, ⁴J(³¹P-¹³C) = 3 Hz, C_{p,P}-phenyl), 129.0 (d, ³J(³¹P-¹³C) = 10 Hz, C_{m,P}-phenyl), 127.2 (d, ¹J(³¹P-¹³C) = 34 Hz, C₆ or C_{i,P}-phenyl), 121.7 (d, ⁵J(³¹P-¹³C) = 7 Hz, C₃), 120.9 (d, ³J(³¹P-¹³C) = 6 Hz, C₈), 118.7 (d, ¹J(³¹P-¹³C) = 36 Hz, C_{i,P}-phenyl or C₆), 31.0 (s, C₁ or C₂), 30.4 ppm (s, C₂ or C₁). ³¹P{¹H} NMR (CDCl₃): δ -42.6 ppm (s, J(^{119/117}Sn-³¹P) = 635/606 Hz). ¹¹⁹Sn{¹H} NMR (CDCl₃): δ -259.7 ppm (d, J(³¹P-¹¹⁹Sn) = 637 Hz). MS (EI⁺): *m/z* 562 [M⁺].

Synthesis of Bis(6-(diphenylphosphino)acenaphth-5-yl)tin Dichloride (6). *n*-Butyllithium (1.20 mmol, 2.5 M in *n*-hexane) and *N,N,N',N'*-tetramethylethylenediamine (0.14 g, 1.20 mmol) were added at -78 °C to a suspension of 5-bromo-6-(diphenylphosphino)acenaphthene (0.50 g, 1.20 mmol) in diethyl ether (5 mL) and stirred for 2 h at this temperature. The suspension was warmed to room temperature, stirred for 1 h, and cooled to -78 °C. Tin(IV) chloride (0.16 g, 0.60 mmol) was slowly added, and the mixture was warmed to room temperature overnight. The precipitate was filtered, washed extensively with diethyl ether, and dried in vacuo. Dichloromethane (50 mL) was added, and the suspension was filtered. The filtrate was reduced until the product started to precipitate (8-10 mL) and stored at 5 °C for further precipitation. The white precipitate was filtered and dried in vacuo, affording 6 as a colorless solid (141 mg, 0.16 mmol, 14%; mp 210 °C dec). Crystals suitable for X-ray crystallography were obtained by recrystallization from dichloromethane under reflux.

¹H NMR (CD₂Cl₂): δ 8.69 (d, ³J(¹H-¹H) = 6 Hz, ³J(^{119/117}Sn-¹H) = 131 Hz, 2H, H-4), 7.61 (d, ³J(¹H-¹H) = 7 Hz, 2H), 7.51-7.44 (m, 5H), 7.42-7.27 (m, 9H), 6.94 (t, ³J(¹H-¹H) = 7 Hz, 2H), 6.61 (t, ³J(¹H-¹H) = 7 Hz, 4H), 6.19 (s, 4H), 3.56 ppm (s, 8H, H-1,2). ¹³C{¹H} NMR (CD₂Cl₂): δ 152.0 (s, C_b or C_c), 149.3 (s, C_c or C_d), 137.8 (s), 135.9 (broad), 133.5, 133.3, 133.2, 133.0, 129.4 (s), 128.5 (very broad), 121.9 (s), 120.4 (s), 31.1 (s, C₁ or C₂), 30.7 ppm (s, C₂ or C₁). ³¹P{¹H} NMR (CD₂Cl₂): δ -45.6 ppm (s, J(^{119/117}Sn-³¹P) = 1011/960 Hz). ESI MS (CH₂Cl₂/MeCN 1/10, positive mode): *m/z* 829.3 (C₄₈H₃₆Cl₂PSn) for [6-(Ph₂P)-5-Ace]₂SnCl₂ - Cl⁻.

Synthesis of (6-(Diphenylphosphino)acenaphth-5-yl)-diphenylstannyl Triflate (7). Trifluoromethanesulfonic acid (22.0 mg, 0.15 mmol) was slowly added to a solution of (6-(diphenylphosphino)acenaphth-5-yl)triphenyltin (2; 100 g, 0.15 mmol) in dichloromethane (1.5 mL), and the reaction mixture was stirred for 12 h. The solvent was evaporated, and the residue was recrystallized by dichloromethane and *n*-hexane, affording 7 as colorless crystals (49.2 mg, 0.06 mmol, 40%; mp 193 °C dec).

^1H NMR (CDCl_3): δ 8.71 (d, $^3J(\text{H}-\text{H}) = 7$ Hz, $^3J(^{119/117}\text{Sn}-\text{H}) = 73$ Hz, 1H, H-4), 7.75 (d, $^3J(\text{H}-\text{H}) = 7$ Hz, 1H), 7.53 (dd, $^3J(\text{H}-\text{H}) = 7$ Hz, $^4J(\text{H}-\text{H}) = 1$ Hz, $^3J(^{119/117}\text{Sn}-\text{H}) = 68$ Hz, 4H, H-C_{o,Sn-phenyl}), 7.47–7.45 (m, 2H), 7.36–7.20 (m, 8H), 7.14 (dt, $^3J(\text{H}-\text{H}) = 8$ Hz, $^4J(\text{H}-\text{H}) = 2$ Hz, H4), 6.88 (t, $^3J(\text{H}-\text{H}) = 9$ Hz, 4H), 3.61–3.54 ppm (m, 4H, H-1,2). $^{13}\text{C}\{^1\text{H}\}$ NMR (CDCl_3): δ 153.0 (d, $J(^{31}\text{P}-^{13}\text{C}) = 2$ Hz, C_b or C_c), 149.6 (d, $J(^{31}\text{P}-^{13}\text{C}) = 2$ Hz, C_c or C_b), 141.1 (d, $^3J(^{31}\text{P}-^{13}\text{C}) = 8$ Hz, C₄), 139.8 (d, $^2J(^{31}\text{P}-^{13}\text{C}) = 9$ Hz, C_a or C₇), 138.0 (d, $J(^{31}\text{P}-^{13}\text{C}) = 23$ Hz, C₅, C₆ or C_{i,P-phenyl}), 136.8 (d, $J(^{31}\text{P}-^{13}\text{C}) = 1$ Hz, C_{i,Sn-phenyl}), 136.2 (d, $J(^{31}\text{P}-^{13}\text{C}) = 2$ Hz, $^2J(^{119/117}\text{Sn}-^{13}\text{C}) = 48$ Hz, C_{o,Sn-phenyl}), 134.1 (d, $^2J(^{31}\text{P}-^{13}\text{C}) = 12$ Hz, C₇ or C_a), 132.8 (d, $^2J(^{31}\text{P}-^{13}\text{C}) = 12$ Hz, C_{o,P-phenyl}), 130.6 (d, $^4J(^{31}\text{P}-^{13}\text{C}) = 2$ Hz, C_{p,P-phenyl}), 129.6 (s, C_{p,Sn-phenyl}), 128.8 (d, $^3J(^{31}\text{P}-^{13}\text{C}) = 10$ Hz, C_{m,P-phenyl}), 128.8 (s, $^3J(^{119/117}\text{Sn}-^{13}\text{C}) = 76/73$ Hz, C_{m,Sn-phenyl}), 126.9 (d, $J(^{31}\text{P}-^{13}\text{C}) = 35$ Hz, C₅, C₆ or C_{i,P-phenyl}), 122.4 (d, $^5J(^{31}\text{P}-^{13}\text{C}) = 4$ Hz, C₃), 121.1 (d, $J(^{31}\text{P}-^{13}\text{C}) = 35$ Hz, C₅, C₆ or C_{i,P-phenyl}), 120.4 (d, $^3J(^{31}\text{P}-^{13}\text{C}) = 6$ Hz, C₈), 30.8 (s, C₁ or C₂), 30.4 ppm (s, C₂ or C₁). $^{31}\text{P}\{^1\text{H}\}$ NMR (CDCl_3): δ -27.0 ppm (s, $J(^{119/117}\text{Sn}-^{31}\text{P}) = 686/656$ Hz). $^{31}\text{P}\{^1\text{H}\}$ NMR (CD_3CN): δ -24.4 ppm (s, $J(^{119/117}\text{Sn}-^{31}\text{P}) = 585/559$ Hz). $^{119}\text{Sn}\{^1\text{H}\}$ NMR (CDCl_3): δ -214.8 ppm (d, $J(^{31}\text{P}-^{119}\text{Sn}) = 687$ Hz). $^{119}\text{Sn}\{^1\text{H}\}$ NMR (CD_3CN): δ -194.9 ppm (d, $J(^{31}\text{P}-^{119}\text{Sn}) = 592$ Hz). ESI MS ($\text{CH}_2\text{Cl}_2/\text{MeCN}$ 1/10, positive mode): m/z 611.3 (C₃₆H₂₈PSn) for $[\text{S}-(\text{SnPh}_2)\text{-6}-(\text{Ph}_2\text{P})\text{Ace}]^+$ (7). Molar conductivity (MeCN , $c = 5 \times 10^{-7}$ mol L⁻¹): Λ 360 Ω^{-1} cm² mol⁻¹.

Synthesis of (6-(Diphenylphosphino)acenaphth-5-yl)-diphenyltin Fluoride (8). To a suspension of potassium fluoride (45.0 mg, 0.77 mmol) and dimethylformamide (3 mL) was slowly added 6-(diphenylphosphino)acenaphth-5-yl)diphenyltin chloride (3; 100 mg, 0.15 mmol), and the reaction mixture was stirred at room temperature overnight. The precipitate was filtered, washed with dimethylformamide (2 mL), and dried in vacuo, yielding **8** as a colorless solid (87.1 mg, 0.14 mmol, 89%; mp 217 °C dec). Crystals suitable for X-ray crystallography were obtained by recrystallization by dimethylformamide.

^1H NMR (CD_2Cl_2): δ 8.60 (d, $^3J(\text{H}-\text{H}) = 7$ Hz, $^3J(^{119/117}\text{Sn}-\text{H}) = 69$ Hz, 1H, H-4), 7.66–7.56 (m, 5H), 7.47–7.17 (m, 10H), 7.11 (dt, $^3J(\text{H}-\text{H}) = 8$ Hz, $^4J(\text{H}-\text{H}) = 2$ Hz, 4H), 6.86 (t, $^3J(\text{H}-\text{H}) = 8$ Hz, 4H), 3.51 ppm (a, 4H, H-1,2). $^{13}\text{C}\{^1\text{H}\}$ NMR (CD_2Cl_2): δ 152.0 (d, $J(^{31}\text{P}-^{13}\text{C}) = 2$ Hz, C_b or C_c), 149.5 (d, $J(^{31}\text{P}-^{13}\text{C}) = 2$ Hz, C_c or C_b), 140.2 (dd, $^3J(^{19}\text{F}-^{13}\text{C}) = 4$ Hz, $^2J(^{31}\text{P}-^{13}\text{C}) = 8$ Hz, C_a), 137.3 (d, $J(^{31}\text{P}$ or $^{19}\text{F}-^{13}\text{C}) = 3$ Hz, C_{i,Sn-phenyl}), 136.6 (d, $J(^{31}\text{P}$ or $^{19}\text{F}-^{13}\text{C}) = 2$ Hz, $^2J(^{119/117}\text{Sn}-^{13}\text{C}) = 43$ Hz, C_{o,Sn-phenyl}), 133.3 (d, $^2J(^{31}\text{P}-^{13}\text{C}) = 14$ Hz, C_{o,P-phenyl}), 132.1 (d, $J(^{31}\text{P}-^{13}\text{C}) = 15$ Hz, C₅, C₆ or C_{i,P-phenyl}), 129.6 (d, $^4J(^{31}\text{P}-^{13}\text{C}) = 1$ Hz, C_{p,P-phenyl}), 129.4 (s, C_{p,Sn-phenyl}), 128.9 (d, $J(^{31}\text{P}-^{13}\text{C}) = 22$ Hz, C₅, C₆ or C_{i,P-phenyl}), 128.8 (s, $^3J(^{119/117}\text{Sn}-^{13}\text{C}) = 70$ Hz, C_{m,Sn-phenyl}), 128.8 (d, $^3J(^{31}\text{P}-^{13}\text{C}) = 8$ Hz, C_{m,P-phenyl}), 125.1 (d, $J(^{31}\text{P}-^{13}\text{C}) = 17$ Hz, C₅, C₆ or C_{i,P-phenyl}), 121.5 (d, $J(^{31}\text{P}$ or $^{19}\text{F}-^{13}\text{C}) = 4$ Hz, C₃), 120.4 (d, $^3J(^{31}\text{P}-^{13}\text{C}) = 4$ Hz, C₈), 30.9 (s, C₁ or C₂), 30.7 ppm (s, C₂ or C₁). $^{19}\text{F}\{^1\text{H}\}$ NMR (CD_2Cl_2): δ -184.9 ppm (d, $J(^{31}\text{P}-^{19}\text{F}) = 84$ Hz, $^1J(^{119/117}\text{Sn}-^{19}\text{F}) = 2232/2133$ Hz). $^{31}\text{P}\{^1\text{H}\}$ NMR (CD_2Cl_2): δ -34.1 ppm (d, $J(^{19}\text{F}-^{31}\text{P}) = 84$ Hz, $J(^{119/117}\text{Sn}-^{31}\text{P}) = 712/678$ Hz). $^{119}\text{Sn}\{^1\text{H}\}$ NMR (CD_2Cl_2): δ -232.4 ppm (dd, $^1J(^{19}\text{F}-^{119}\text{Sn}) = 2232$ Hz), $J(^{31}\text{P}-^{119}\text{Sn}) = 714$ Hz). MS (EI^+): m/z : 611 [(M - F)⁺].

X-ray Crystallography. Intensity data were collected on a STOE IPDS 2T area detector (1, 3–5, 7, 8) and a Siemens P4 diffractometer (1, 2, 6) at 173 K with graphite-monochromated Mo K α (0.7107 Å) radiation. All structures were solved by direct methods and refined based on F^2 by use of the SHELX program package.⁴⁶ All non-hydrogen atoms were refined using anisotropic displacement parameters. Hydrogen atoms attached to carbon atoms were included in geometrically calculated positions using a riding model. Crystal and refinement data are collected in Table S1 (Supporting Information). Figures were created using DIAMOND.⁴⁷ Crystallographic data (excluding structure factors) for the structural analyses have been deposited with the Cambridge Crystallographic Data Centre, CCDC nos. 985248–985255 (1–8). Copies of this information may be obtained free of charge from The Director, CCDC, 12 Union Road,

Cambridge CB2 1EZ, U.K. (fax, +44-1223-336033; e-mail, deposit@ccdc.cam.ac.uk; web, <http://www.ccdc.cam.ac.uk>).

Computational Methodology. Gas-phase structures of 2–5 and 7a,b were obtained by geometry optimization at the B3PW91/6-311+G(2df,p)³⁵ level of theory starting from the atomic coordinates of the X-ray structures using Gaussian09.⁴⁸ For the Sn atom an effective core potential (ECP28MDF)⁴⁹ and a corresponding cc-pVTZ basis set⁵⁰ were applied. Subsequent frequency analysis proves all structures to be local minima. The wave function files were used for a topological analysis of the electron density (ED) according to the atoms in molecules space-partitioning scheme¹⁶ using AIM2000,³⁸ whereas DGRID⁵¹ was used to generate and analyze the electron localizability indicator (ELI-D) related real-space bonding descriptors, applying a grid step size of 0.05 au.¹⁷

■ ASSOCIATED CONTENT

Supporting Information

Figures, tables, and CIF files giving NMR spectra of 1–8, crystallographic data for 1–8, crystal data and structure refinement details for 1–8, selected ELI-D properties of 2–8, AIM bond paths and isosurface representations of the localization domains of the ELI-D ($Y = 1.4$) of 3, 4, 8, 2 (experimental geometry), Ph₃Sn⁺, and Ph₃SnCl, ELI-D distribution mapped on the Sn–P basin of 3, 4, 8, and the P lone pair basin of 2 (experimental geometry), and Cartesian coordinates of the optimized gas-phase structures of 2–5, 7a,b, and 8. This material is available free of charge via the Internet at <http://pubs.acs.org>.

■ AUTHOR INFORMATION

Notes

The authors declare no competing financial interest.

■ ACKNOWLEDGMENTS

The Deutsche Forschungsgemeinschaft (DFG) is gratefully acknowledged for financial support. We indebted to Prof. Dr. Takahiro Sasamori, Kyoto University, for valuable comments on the NMR parameters. Dedicated to Prof. Dr. Gerd-Volker Röschenhalter on the occasion of his 70th birthday.

■ REFERENCES

- (1) (a) Hoefelmeyer, J. D.; Schulte, M.; Tschinkl, M.; Gabbai, F. P. *Coord. Chem. Rev.* **2002**, *235*, 93–103. (a) Kilian, P.; Knight, F. R.; Woollins, J. D. *Chem. Eur. J.* **2011**, *17*, 2302–2328.
- (2) (a) Sooriyakumaran, R.; Boudjouk, P. *Organometallics* **1982**, *1*, 218–219. (b) Sooriyakumaran, R.; Boudjouk, P.; Garvey, R. G. *Acta Crystallogr., Sect. C* **1985**, *C41*, 1348–1350.
- (3) Jackson, R. D.; James, S.; Orpen, A. G.; Pringle, P. G. *J. Organomet. Chem.* **1993**, *458*, C3–C4.
- (4) Wawrzyniak, P.; Fuller, A. L.; Slawin, A. M. Z.; Kilian, P. *Inorg. Chem.* **2009**, *48*, 2500–2506.
- (5) Li, Y.-F.; Kang, Y.; Ko, S.-B.; Rao, Y.; Sauriol, F.; Wang, S. *Organometallics* **2013**, *32*, 3063–3068.
- (6) (a) Beckmann, J.; Hupf, E.; Lork, E.; Mebs, S. *Inorg. Chem.* **2013**, *52*, 11881–11888. (b) Bontemps, S.; Devillard, M.; Mallet-Ladeira, S.; Bouhadir, G.; Miqueu, K.; Bourissou, D. *Inorg. Chem.* **2013**, *52*, 4714–4720. (c) Li, Y.-F.; Kang, Y.; Ko, S.-B.; Rao, Y.; Sauriol, F.; Wang, S. *Organometallics* **2013**, *32*, 3063–3068. (d) Tsurusaki, S.; Sasamori, T.; Wakamiya, A.; Yamaguchi, S.; Nagura, K.; Irle, S.; Tokitoh, N. *Angew. Chem.* **2011**, *123*, 11132–11135; *Angew. Chem., Int. Ed.* **2011**, *50*, 10940–10943. (e) Sasamori, T.; Tsurusaki, A.; Tokitoh, N.; Wakamiya, A.; Nagura, K.; Irle, S.; Yamaguchi, S. Oral presentation No. O21, 13th International Symposium of Inorganic Ring Systems (IRIS 13), Victoria, British Columbia, Canada, July 29–August 2, 2012.

- (7) Hounshell, W. D.; Anet, F. A. L.; Cozzi, F.; Damewood, J. R.; Johnson, C. A.; Sjostrand, U.; Mislow, K. *J. Am. Chem. Soc.* **1980**, *102*, 5941–5942.
- (8) (a) Jastrzebski, J. T. B. H.; Knaap, C. T.; van Koten, G. *J. Organomet. Chem.* **1983**, *255*, 287–293. (b) Jastrzebski, J. T. B. H.; Grove, D. M.; Boersma, J.; van Koten, G.; Ernsting, J.-M. *Magn. Reson. Chem.* **1991**, *29*, 25–30. (c) Jastrzebski, J. T. B. H.; Boersma, J.; Esch, P. M.; van Koten, G. *Organometallics* **1991**, *10*, 930–935. (d) Jastrzebski, J. T. B. H.; van der Schaaf, P. A.; Boersma, J.; van Koten, G.; de Wit, M.; Wang, Y.; Heijdenrijk, D.; Stam, C. H. *J. Organomet. Chem.* **1991**, *407*, 301–311. (e) Jastrzebski, J. T. B. H.; van der Schaaf, P. A.; Boersma, J.; van Koten, G.; de Ridder, D. J. A.; Heijdenrijk, D. *Organometallics* **1992**, *11*, 1521–1526.
- (9) Lechner, M.-L.; Arachchige, K. S. A.; Randall, R. A. M.; Knight, F. R.; Bühl, M.; Slawin, A. M. Z.; Woollins, J. D. *Organometallics* **2012**, *31*, 2922–2930.
- (10) (a) van Koten, G.; Noltes, J. G.; Spek, A. L. *J. Organomet. Chem.* **1976**, *118*, 183–189. (b) van Koten, G.; Jastrzebski, J. T. B. H.; Noltes, J. G.; Spek, A. L.; Schoone, J. C. *J. Organomet. Chem.* **1978**, *148*, 233–245. (c) van Koten, G.; Jastrzebski, J. T. B. H.; Noltes, J. G.; Pontenagel, W. M. G. F.; Kroon, J.; Spek, A. L. *J. Am. Chem. Soc.* **1978**, *100*, 5021–5028. (d) van Koten, G.; Jastrzebski, J. T. B. H.; Noltes, J. G. *J. Organomet. Chem.* **1979**, *177*, 283–292. (e) Jurkschat, K.; Kalbitz, J.; Dargatz, M.; Kleinpeter, E.; Tzschach, A. *J. Organomet. Chem.* **1988**, *347*, 41–57. (f) Jastrzebski, J. T. B. H.; van der Schaaf, P. A.; Boersma, J.; van Koten, G.; Zoutberg, M. C.; Heijdenrijk, D. *Organometallics* **1989**, *8*, 1373–1375. (g) Jastrzebski, J. T. B. H.; Boersma, J.; Van Koten, G. *J. Organomet. Chem.* **1991**, *413*, 43–53. (h) Schollmeyer, D.; Hartung, H.; Klaus, C.; Jurkschat, K. *Main Group Met. Chem.* **1991**, *14*, 27–32. (i) Dakternieks, D.; Dyson, G.; Jurkschat, K.; Tozer, R.; Tiekink, E. R. T. *J. Organomet. Chem.* **1993**, *458*, 29–38. (j) Kolb, U.; Dräger, M.; Dargatz, M.; Jurkschat, K. *Organometallics* **1995**, *14*, 2827–2834. (k) Pieper, N.; Klaus-Mrestani, C.; Schürmann, M.; Jurkschat, K.; Biesemans, M.; Verbruggen, I.; Martins, J. C.; Willem, R. *Organometallics* **1997**, *16*, 1043–1052. (l) Steenwinkel, P.; Jastrzebski, J. T. B. H.; Deelman, B.-J.; Grove, D. M.; Kooijman, H.; Veldman, N.; Smeets, W. J. J.; Spek, A. L.; van Koten, G. *Organometallics* **1997**, *16*, 5486–5498. (m) Schwarzkopf, K.; Metzger, J. O.; Saak, W.; Pohl, S. *Chem. Ber.* **1997**, *130*, 1539–1546. (n) Mehring, M.; Schürmann, M.; Jurkschat, K. *Organometallics* **1998**, *17*, 1227–1236. (o) Mehring, M.; Löw, C.; Schürmann, M.; Jurkschat, K. *Eur. J. Inorg. Chem.* **1999**, *5*, 887–898. (p) Rippstein, R.; Kickelbick, G.; Schubert, U. *Monatsh. Chem.* **1999**, *130*, 385–399.
- (11) (a) Mehring, M.; Vrasidas, I.; Horn, D.; Schürmann, M.; Jurkschat, K. *Organometallics* **2001**, *20*, 4647–4653. (b) Jurkschat, K.; Pieper, N.; Seemeyer, S.; Schürmann, M.; Biesemans, M.; Verbruggen, I.; Willem, R. *Organometallics* **2001**, *20*, 868–880. (c) Jambor, R.; Ruzicka, A.; Brus, J.; Cisarova, I.; Holecek, J. *Inorg. Chem. Commun.* **2001**, *4*, 257–260. (d) Jambor, R.; Dostal, L.; Ruzicka, A.; Cisarova, I.; Brus, J.; Holcapek, M.; Holecek, J. *Organometallics* **2002**, *21*, 3996–4004. (e) Peveling, K.; Henn, M.; Löw, C.; Mehring, M.; Schürmann, M.; Costisella, B.; Jurkschat, K. *Organometallics* **2004**, *23*, 1501–1508. (f) Kasna, B.; Jambor, R.; Dostal, L.; Ruzicka, A.; Cisarova, I.; Holecek, J. *Organometallics* **2004**, *23*, 5300–5307. (g) Bares, J.; Novak, P.; Nadvornik, M.; Jambor, R.; Lebl, T.; Cisarova, I.; Ruzicka, A.; Holecek, J. *Organometallics* **2004**, *23*, 2967–2971. (h) Novak, P.; Brus, J.; Cisarova, I.; Ruzicka, A.; Holecek, J. *J. Fluorine Chem.* **2005**, *126*, 1531–1538. (i) Novak, P.; Padelkova, Z.; Kolarova, L.; Cisarova, I.; Ruzicka, A.; Holecek, J. *Appl. Organomet. Chem.* **2005**, *19*, 1101–1108. (j) Lebl, T.; Zoufala, P.; Bruhn, C. *Eur. J. Inorg. Chem.* **2005**, *12*, 2536–2544. (k) Blanka, K.; Jambor, R.; Dostal, L.; Kolarova, L.; Cisarova, I.; Holecek, J. *Organometallics* **2006**, *25*, 148–153. (l) Fischer, J.; Schürmann, M.; Mehring, M.; Zachwieja, U.; Jurkschat, K. *Organometallics* **2006**, *25*, 2886–2893. (m) Kasna, B.; Jambor, R.; Dostal, L.; Cisarova, I.; Holecek, J. *J. Organomet. Chem.* **2006**, *691*, 1554–1559. (n) Novak, P.; Cisarova, I.; Kolarova, L.; Ruzicka, A.; Holecek, J. *J. Organomet. Chem.* **2007**, *692*, 4287–4296. (o) Kasna, B.; Dostal, L.; Jirasko, R.; Cisarova, I.; Jambor, R. *Organometallics* **2008**, *27*, 3743–3747. (p) Padelkova, Z.; Nechaev, M. S.; Cernosek, Z.; Brus, J.; Ruzicka, A. *Organometallics* **2008**, *27*, 5303–5308. (q) Svec, P.; Eisner, A.; Kolarova, L.; Weidlich, T.; Pejchal, V.; Ruzicka, A. *Tetrahedron Lett.* **2008**, *49*, 6320–6323. (r) Rotar, A.; Schürmann, M.; Varga, R. A.; Silvestru, C.; Jurkschat, K. *Z. Anorg. Allg. Chem.* **2008**, *634*, 1533–1536. (s) Varga, R. A.; Jurkschat, K.; Silvestru, C. *Eur. J. Inorg. Chem.* **2008**, *5*, 708–716. (t) Rotar, A.; Varga, R. A.; Jurkschat, K.; Silvestru, C. *J. Organomet. Chem.* **2009**, *694*, 1385–1392. (u) Padelkova, Z.; Vankatova, H.; Cisarova, I.; Nechaev, M. S.; Zevaco, T. A.; Walter, O.; Ruzicka, A. *Organometallics* **2009**, *28*, 2629–2632.
- (12) (a) Turek, J.; Padelkova, Z.; Nechaev, M. S.; Ruzicka, A. *J. Organomet. Chem.* **2010**, *695*, 1843–1847. (b) Svec, P.; Cernoskova, E.; Padelkova, Z.; Ruzicka, A.; Holecek, J. *J. Organomet. Chem.* **2010**, *695*, 2475–2485. (c) Mairychova, B.; Dostal, L.; Ruzicka, A.; Fulem, M.; Ruzicka, K.; Lycka, A.; Jambor, R. *Organometallics* **2011**, *30*, 5904–5910. (d) Mairychova, B.; Dostal, L.; Ruzicka, A.; Benes, L.; Jambor, R. *J. Organomet. Chem.* **2012**, *699*, 1–4. (e) Wagner, M.; Dietz, C.; Bouska, M.; Dostal, L.; Padelkova, Z.; Jambor, R.; Jurkschat, K. *Organometallics* **2013**, *32*, 4973–4984.
- (13) Britton, D.; Dunitz, J. D. *J. Am. Chem. Soc.* **1981**, *103*, 2971–2979.
- (14) (a) Suzuki, M.; Son, I.-H.; Noyori, R.; Masuda, H. *Organometallics* **1990**, *9*, 3043–3053. (b) Akiba, K.-y. *Organometallics*; Wiley: Hoboken, NJ, 2011. (c) Ponec, R.; Yuzhakov, G.; Cooper, D. L. *Theor. Chem. Acc.* **2004**, *112*, 419–430.
- (15) (a) Grabowski, S. J. *Phys. Chem. Chem. Phys.* **2014**, *16*, 1824–1834. (b) Murray, J. S.; Riley, K. E.; Politzer, P.; Clark, T. *Aus. J. Chem.* **2010**, *63*, 1598–1607. (c) Mikosch, J.; Trippel, S.; Eichhorn, C.; Otto, R.; Lourderaj, U.; Zhang, J. X.; Hase, W. L.; Weidemüller, M.; Wester, R. *Science* **2008**, *319*, 183–186. (d) Bento, A. P.; Bickelhaupt, F. M. *J. Org. Chem.* **2007**, *72*, 2201–2207.
- (16) Bader, R. W. F. *Atoms in Molecules: A Quantum Theory*; Cambridge University Press: Oxford U.K., 1991.
- (17) (a) Koritsanszky, T.; Coppens, P. *Chem. Rev.* **2001**, *101*, 1583–1628. (b) Macchi, P.; Sironi, A. *Coord. Chem. Rev.* **2003**, *238*–239, 383–412. (c) Gatti, C. *Z. Kristallogr.* **2005**, *220*, 399–457.
- (18) (a) Becke, A. D.; Edgecombe, K. E. *J. Chem. Phys.* **1990**, *92*, 5397–5403. (b) Silvi, B.; Savin, A. *Nature* **1994**, *371*, 683–686.
- (19) (a) Kohout, M. *Int. J. Quantum Chem.* **2004**, *97*, 651–658. (b) Kohout, M.; Wagner, F. R.; Grin, Y. *Theor. Chem. Acc.* **2008**, *119*, 413–420.
- (20) (a) Raub, S.; Jansen, G. *Theor. Chem. Acc.* **2001**, *106*, 223–232. (b) Vidal, I.; Melchor, S.; Dobado, J. A. *J. Phys. Chem. A* **2005**, *109*, 7500–7508.
- (21) (a) Mebs, S.; Grabowsky, S.; Förster, D.; Kickbusch, R.; Hartl, M.; Daemen, L. L.; Morgenroth, W.; Luger, P.; Paulus, B.; Lentz, D. *J. Phys. Chem. A* **2010**, *114*, 10185–10196. (b) Mebs, S.; Kalinowski, R.; Grabowsky, S.; Förster, D.; Kickbusch, R.; Justus, E.; Morgenroth, W.; Paulmann, C.; Luger, P.; Gabel, D.; Lentz, D. *J. Phys. Chem. A* **2011**, *115*, 1385–1395.
- (22) Part of this work was presented at the 14th International Conference on the Coordination and Organometallic Chemistry of Germanium, Tin and Lead (GTL-14), book of abstracts, poster no. P9; Baddeck, Cape Breton Island, Nova Scotia, Canada, July 14–19, 2013.
- (23) (a) Dräger, M. *Z. Anorg. Allg. Chem.* **1976**, *423*, 53–66. (b) Kolb, U.; Beuter, M.; Dräger, M. *Inorg. Chem.* **1994**, *33*, 4522–4530.
- (24) Reuter, H.; Puff, H. *J. Organomet. Chem.* **1989**, *379*, 233–234.
- (25) Zickgraf, A.; Beuter, M.; Kolb, U.; Dräger, M.; Tozer, R.; Dakternieks, D.; Jurkschat, K. *Inorg. Chim. Acta* **1998**, *275*–276, 203–214.
- (26) Beckmann, J.; Lork, E.; Mallow, O. *Main Group Met. Chem.* **2012**, *35*, 183–185.
- (27) Westerhausen, M.; Schwarz, W. *Main Group Met. Chem.* **1997**, *20*, 351–359.
- (28) Tudela, D.; Gutiérrez-Puebla, E.; Monge, A. *J. Chem. Soc., Dalton Trans.* **1992**, 1069–1071.

- (29) Beckmann, J.; Dakternieks, D.; Duthie, A.; Tiekink, E. R. T. *J. Organomet. Chem.* **2002**, *648*, 204–208.
- (30) Freitag, S.; Krebs, K. M.; Henning, J.; Hirdler, J.; Schubert, H.; Wesemann, L. *Organometallics* **2013**, *32*, 6785–6791.
- (31) Geary, W. J. *Coord. Chem. Rev.* **1971**, *7*, 81–122.
- (32) (a) Ng, S.; Sathasivam, R. V.; Lo, K.-H.; Xie, Y.; Schaefer, H. F. *J. Phys. Chem. A* **2005**, *109*, 12059–12603. (b) Davies, A. G.; Harrison, P. G.; Kennedy, J. D.; Mitchell, T. N.; Puddephatt, R. J.; McFarlane, N. *J. Chem. Soc. C* **1969**, 1136–1141.
- (33) Bühl, M.; Knight, F. R.; Krístková, A.; Ondík, I. M.; Malkina, O. L.; Randall, R. A. M.; Slawin, A. M. Z.; Woollins, J. D. *Angew. Chem., Int. Ed.* **2013**, *52*, 2495–2498.
- (34) Beckmann, J.; Horn, D.; Jurkschat, K.; Rosche, F.; Schürmann, M.; Zachwieja, U.; Dakternieks, D.; Duthie, A.; Lim, A. E. K. *Eur. J. Inorg. Chem.* **2003**, 164–174.
- (35) (a) Perdew, J. P.; Chevary, J. A.; Vosko, S. H.; Jackson, K. A.; Pederson, M. R.; Singh, D. J.; Fiolhais, C. *Phys. Rev. B* **1992**, *46*, 6671–6687. (b) Becke, A. D. *J. Chem. Phys.* **1993**, *98*, 5648–5652.
- (36) Beckmann, J.; Do, T. G.; Grabowsky, S.; Hupf, E.; Lork, E.; Mebs, S. Z. *Anorg. Allg. Chem.* **2013**, *639*, 2233–2249.
- (37) Keller, E. SCHAKAL; Albert Ludwigs Universität, Freiburg, Germany, 1999.
- (38) Biegler-König, F.; Schönbohm, J.; Bayles, D. J. *Comput. Chem.* **2001**, *22*, 545–559.
- (39) Vidal, I.; Melchor, S.; Dobado, J. A. *J. Phys. Chem. A* **2005**, *109*, 7500–7508.
- (40) Mebs, S.; Chilleck, M.; Grabowsky, S.; Braun, T. *Chem. Eur. J.* **2012**, *18*, 11647–11661.
- (41) Hübschle, C. B.; Luger, P. *J. Appl. Crystallogr.* **2006**, *39*, 901–904.
- (42) Beckmann, J.; Bolsinger, J.; Finke, P.; Lork, E.; Lüdke, C.; Mallow, O.; Mebs, S. *Inorg. Chem.* **2012**, *51*, 12395–12406.
- (43) Beckmann, J.; Heinrich, D.; Mebs, S. Z. *Anorg. Allg. Chem.* **2013**, *639*, 2129–2133.
- (44) Himmel, D.; Krossing, I.; Schnepf, A. *Angew. Chem., Int. Ed.* **2014**, *53*, 370–374.
- (45) (a) Jurkschat, K.; Abicht, H. P.; Tzschach, A.; Mahieu, B. *J. Organomet. Chem.* **1986**, *309*, C47–C50. (b) Hoppe, S.; Weichmann, H.; Jurkschat, K.; Schneider-Koglin, C.; Dräger, M. *J. Organomet. Chem.* **1995**, *505*, 63–72. (c) Steinborn, D.; Neumann, O.; Weichmann, H.; Heinemann, F. W.; Wagner, J.-P. *Polyhedron* **1997**, *17*, 351–355. (d) Kruber, D.; Merzweiler, K.; Wagner, C.; Weichmann, H. *J. Organomet. Chem.* **1999**, *572*, 117–123. (e) Baumeister, U.; Hartung, H.; Krug, A.; Merzweiler, K.; Schulz, T.; Wagner, C.; Weichmann, H. *Z. Anorg. Allg. Chem.* **2000**, *626*, 2185–2195. (f) Seibert, M.; Merzweiler, K.; Wagner, C.; Weichmann, H. *J. Organomet. Chem.* **2002**, *650*, 25–36. (g) Seibert, M.; Merzweiler, K.; Wagner, C.; Weichmann, H. *J. Organomet. Chem.* **2003**, *687*, 131–141. (h) Lin, T.-P.; Gualco, P.; Ladeira, S.; Amgoune, A.; Maron, L.; Gabbai, F. P.; Bourissou, D. *C. R. Chim.* **2010**, *13*, 1168–1172.
- (46) Sheldrick, G. M. A short history of SHELX. *Acta Crystallogr., Sect. A* **2008**, *A64*, 112–122.
- (47) Brandenburg, K.; Putz, H. *DIAMOND V3.1d*; Crystal Impact GbR, 2006.
- (48) Frisch, M. J.; Trucks, G. W.; Schlegel, H. B.; Scuseria, G. E.; Robb, M. A.; Cheeseman, J. R.; Scalmani, G.; Barone, V.; Mennucci, B.; Petersson, G. A.; Nakatsuji, H.; Caricato, M.; Li, X.; Hratchian, H. P.; Izmaylov, A. F.; Bloino, J.; Zheng, G.; Sonnenberg, J. L.; Hada, M.; Ehara, M.; Toyota, K.; Fukuda, R.; Hasegawa, J.; Ishida, M.; Nakajima, T.; Honda, Y.; Kitao, O.; Nakai, H.; Vreven, T.; Montgomery, J. A., Jr.; Peralta, J. E.; Ogliaro, F.; Bearpark, M.; Heyd, J. J.; Brothers, E.; Kudin, K. N.; Staroverov, V. N.; Kobayashi, R.; Normand, J.; Raghavachari, K.; Rendell, A.; Burant, J. C.; Iyengar, S. S.; Tomasi, J.; Cossi, M.; Rega, N.; Millam, J. M.; Klene, M.; Knox, J. E.; Cross, J. B.; Bakken, V.; Adamo, C.; Jaramillo, J.; Gomperts, R.; Stratmann, R. E.; Yazyev, O.; Austin, A. J.; Cammi, R.; Pomelli, C.; Ochterski, J. W.; Martin, R. L.; Morokuma, K.; Zakrzewski, V. G.; Voth, G. A.; Salvador, P.; Dannenberg, J. J.; Dapprich, S.; Daniels, A. D.; Farkas, Ö.;
- Foresman, J. B.; Ortiz, J. V.; Cioslowski, J.; Fox, D. J. *Gaussian 09, Revision B.01*; Gaussian, Inc., Wallingford, CT, 2009.
- (49) Metz, B.; Stoll, H.; Dolg, M. *J. Chem. Phys.* **2000**, *113*, 2563–2569.
- (50) Peterson, K. A. *J. Chem. Phys.* **2003**, *119*, 11099–11112.
- (51) Kohout, M. *DGRID, version 4.5*; Radebeul, 2009.